# Development of biomass derived highly porous fast adsorbents for post-combustion $CO_2$ capture

Farooq Sher[a,*], Sania Zafar Iqbal[b], Shaima Albazzaz[c,d], Usman Ali[e], Daniela Andresa Mortari[f], Tazien Rashid[g,h]

*a. School of Mechanical, Aerospace and Automotive Engineering, Faculty of Engineering, Environmental and Computing, Coventry University, Coventry CV1 2JH, UK*
*b. Department of Biochemistry, University of Agriculture, Faisalabad 38000, Pakistan*
*c. Department of Chemical and Environmental Engineering, University of Nottingham, University Park, Nottingham NG7 2RD, UK*
*d. Department of Chemical Engineering, University of Basrah, Basrah, Iraq*
*e. Department of Chemical Engineering, University of Engineering and Technology, Lahore 54890, Pakistan*
*f. São Carlos School of Engineering, University of São Paulo (USP), São Carlos, SP, Brazil*
*g. Department of Chemical Engineering, NFC Institute of Engineering and Fertilizer Research Faisalabad, Pakistan*
*h. Department of Chemical Engineering, Universiti Teknologi Petronas, Bandar Seri Iskandar, Tronoh 32610, Perak, Malaysia*

*Corresponding author:

Dr Farooq Sher
Lecturer
School of Mechanical, Aerospace and Automotive Engineering
Faculty of Engineering, Environmental and Computing
Coventry University
Coventry
CV1 2JH
UK

E-mail address: Farooq.Sher@coventry.ac.uk, Farooq.Sher@gmail.com (F.Sher)
Tel.: +44 (0) 24 7765 7754

# Abstract

This study is carried out for the comparative screening of three groups of biomasses; soft or non-woody (peanut shell); intermediate woody (walnut shell) and hard woody (pine wood) for the development of adsorbents/activated carbons for post-combustion $CO_2$ capture (over $N_2$ balance). Three different groups of biomass residues are selected to study the role and nature of the material in adsorption and selection of the raw material for $CO_2$ adsorbents synthesis for future researches because of the hot issue of anthropogenic $CO_2$ adsorption. The adsorption isotherms studied by the thermal gravimetric analyser (TGA) revealed that $CO_2$ adsorption capabilities in the range of 2.53–3.92 mmol/g (over $N_2$ balance) at 25 $^oC$. The newly synthesised activated carbons (ACs) exhibited a fast rate of adsorption as 41–94% in the initial 2 minutes. Porous surface development with catalytic KOH activation is seen clearly through SEM surface morphological analyses and mathematically confirmed from $S_{BET}$ ranges from 146.86 to 944.05 $m^2/g$. FTIR and XRD peaks verify the generation of basic or inorganic $O_2$-rich moieties, help in acidic $CO_2$ capture. It has been observed from adsorption isotherms that the order of higher adsorption groups is as; peanut shell > pine wood > walnut shell, while the best activation ratio (sample/KOH) is 1:3. The synthesised low cost ACs, with an amount of 1.93 US$ per kg production will help to overcome the environmental hazards and problems caused by $CO_2$ and biomass waste respectively.

**Keywords:** $CO_2$ capture; Biomass waste; Green activated carbons; Adsorption; KOH-activation; Microporous materials and Global warming.

# 1 Introduction

Because of the human activities, there is a noticeable increase observed in the warming of the earth atmosphere and expected to continue throughout the present century as of industrial development. This rapid progress of modern civilization is a primary cause of $CO_2$ emission to the environment. Anthropogenic $CO_2$ from greenhouse gases is a contributor to global warming that is mostly discharged from fossil fuels combustion. Currently, the use of fossil fuels as an energy resource continues to increase especially in developing countries, this is due to the availability of fossil fuels at a reasonable cost [1, 2]. Literature confirmed the increment of > 30 billion tons of $CO_2$ to the atmosphere per year [3]. $CO_2$ emission with this rate has upraised numerous alarms including urban smog, health issues as well as acid rain. Therefore, it is an urgent need of the hour to stabilise the level of this anthropogenic greenhouse pollutant ($CO_2$) before the extensive destruction. Consequently, in the presence of continuous climate change, the European Commission has decided to lessen its carbon discharge by 20–95% between 2020–2050, with reference to 1990 levels [4]. It is cleared in present energy setups of fossil fuels consumption, that the implementation of $CO_2$ capture and its storage (CCS) technologies will display an essential part to achieve the necessary reduction in its emission, to avoid irreversible and eternal destruction to the atmosphere [5-7].

At present, a total three technologies have been introduced for CCS: pre-combustion capture, post-combustion capture and oxy-fuel process. Post-combustion CSS technology can be simply retrofitted to present-day power stations, petrochemical and gas industries, oil refineries and cement industries which worldwide accounts for nearly half of the $CO_2$ emission [8, 9]. Various separation techniques are available for post-combustion capture which includes absorption, cryogenic separation, adsorption and membrane [10, 11]. The physical technique proved to be effective for the separation and purification of gas is adsorption. In adsorption technique, the solid sorbents used for capturing $CO_2$ have potential advantages over other conventional capturing treatment techniques including greater capacity, ease of handling, selectivity and reduced energy for regeneration.

Adsorption method is costly, therefore, utilizing cheap materials for adsorbent preparation makes the method worthwhile. These materials include forestry wastes, agricultural residues and sewage sludge, the first two precursors have more carbon and very less ash content [12]. Different fruit stones; by-products are of special concern collected from food processing units, in quantities enough for obtaining worthy carbon adsorbents with a better regular porous surface and appreciable hardness. Peach stones, apricot stones [13], olive stones [14], cherry stones [15] and grapestones [16] have been used as raw materials for the fabrication of activated adsorbents with high porosity and surface areas. Coconut shells have also been used for the fabrication of microporous adsorbents [17].

Activation of biomass is achieved by two methods; chemical activation and physical activation. The chemical activation method has some benefits on physical activation method. Firstly, it is a single step carbonization followed by activation with an activating agent, and secondly, it is performed at a lower temperature as compared to physical activation [18]. The chemical activation procedure is associated with precursor material impregnation with activating agents (NaOH, KOH, $ZnCl_2$ or salts) then carbonized under inert pressure and finally washed to remove chemicals so that porous structure is left behind. Carbon adsorbents have been used for the treatment of industrial wastewater, removal of organic and inorganic pollutants from flue gases, in addition to the applications of activated carbon are as an adsorbent for $CO_2$ removal [12]. $CO_2$ adsorbents had been prepared from different starting materials other than biomass-based residues and by-products. A group of researchers prepared $CO_2$ adsorbents by KOH activation of petroleum pitch precursor [19]. The fabricated material exhibited an outstanding adsorption potential for $CO_2$ with values as high as 380 mg $CO_2$ g/sorbent at 0 $^oC$ temperature and 1 bar pressure. Nitrogen enriched $CO_2$ adsorbents have also been prepared from formaldehyde-urea resin by chemical activation with KOH [20]. For these nitrogen enriched activated carbons (ACs), the $CO_2$ adsorption limit is 1.40 mmol/g at 30 $^oC$ temperature under 12.5% $CO_2$ flow. Recently, a study is carried out to analyse the effects of $CO_2$ adsorption by ACs, in terms of power loss and thermal efficiency. Upon comparison, it is concluded that ACs are more advantageous than the commercial adsorbents in rapports of cost and efficiency [21].

In the present study, different groups of biomass residues have been selected to study the role and nature of the material in the post-combustion $CO_2$ adsorption. In addition to this, as the ACs have been prepared by using biomass residues, therefore, this synthesis will be helpful to reduce the landfill space, overcome the pollution and environmental issues caused by $CO_2$ emission. The importance of this study over others is the diverse nature of biomass residues and their activation with a wide range of catalytic KOH. This research has also identified that which activation ratio is important in each group that is helpful for developing interesting surface chemistry, consistent morphology and porous surface structure with excellent surface parameters. The calculation of cost estimation for the production of per kg of ACs has also been done, in order to verify the cheapness of these adsorbents.

# 2 Experimental

Total of twelve ACs have been prepared. The thermal gravimetric analyser (TGA) is used to study the $CO_2$ adsorption (over $N_2$ balance) of synthesised ACs. TGA results helped in the selection of the best samples from each group for further testing.

## 2.1 Synthesis of activated carbons

Biomass product; pine wood (PW) and by-products; peanut shell (PN) and walnut shell (NS) were selected as materials for the preparation of ACs. Pine wood was produced in the United Kingdom while the other two biomasses were obtained from a local supermarket. First raw materials (PW, PS and WS) were crushed, then sieved to particles of size 1 mm for further treatment. Potassium hydroxide (KOH) of 99% concentration (conc.) used as an activating agent was purchased from Sigma-Aldrich.

Biomass-based activated carbons (ACs) were prepared using the single-step chemical activation process, which can successfully develop potassium moieties on raw materials. In this protocol, 3 grams of prepared raw material (PW, PN and NS) samples were first mixed physically with KOH (99% conc.) at different mass ratios including; 1:1, 1:2, 1:3 and 1:4 of raw sample/ KOH (m/m). The physically mixed mixture (raw sample/KOH) was then heated in a horizontal assembly of the furnace tube. The activation of ACs was carried out at 750 $^{o}$C temperature, 5 °C/min heating rate in the presence of 1 L/min nitrogen flow [4].

When the reaction was reached at a specific temperature, the reaction mixture was kept at this temperature for 1 hour, before it was cool down in nitrogen ($N_2$) to ambient conditions. All the time, the neutral gas ($N_2$) was flowing inside the reaction furnace at 1 L/min flow rate. To get final products of ACs, mixtures were removed from the furnace, cool down to room temperature and then washed until neutral with distilled water (usually 3 times washing through 200 mL of water). For the ease of later discussion, twelve synthesised activated carbons are labelled according to their precursor and mass ratio of activation agent as shown in Table 1.

## 2.2 $CO_2$ adsorption

$CO_2$ capture/adsorption measurements of samples (ACs) were carried out using thermogravimetric analysis (TGA, Q500, TA Instruments). For the Individual measurement of $CO_2$ uptake, the sample was first dried at 120 °C in the presence of neutral $N_2$ gas for 1/2 hour to eliminate any possible physisorbed $CO_2$ and/or the moisture content. Then the temperature was lowered to 25 $^{o}$C; adsorption temperature and stabilized. The reaction environment inside the reaction sample chamber was switched to flue gas (15% $CO_2$ in $N_2$) from $N_2$ at 100 mL/min flow rate, at the above set adsorption's temperature for 1 hour. At last, the weight of final sample (AC) was noted to estimate the $CO_2$ uptake. $CO_2$ adsorption measurements were performed to analyze the ACs/adsorbents' surface affinity for $CO_2$ [22].

## 2.3 Characterisation

Ultimate analysis of the biomass samples was determined using a Flash EA 1112 elemental analyzer. Proximate analysis was obtained using the same TGA Q-500 instrument, by heating the sample (s) in $N_2$ at 10 to 110 $^{o}$C/min flow rate. These conditions were maintained for 10 minutes to obtain the moisture content.  The temperature was then increased from 110 to 700 $^{o}$C at 20 $^{o}$C/min flow rate (under $N_2$) and kept for 30 minutes at these conditions to get the weight loss due to this devolatilisation zone after this temperature was ramped at the same rate 20 to 950 $^{o}$C/min. The reaction environment was then switched from $N_2$ to air, inside the furnace compartment and kept it isothermal for 40 minutes to oxidise the char completely to obtain the fixed carbon and ash contents [23]. The results of different weight percentages of fixed carbon (FC), ash, volatile matter (VM), carbon (C), nitrogen (N), hydrogen (H) and oxygen (O) of raw precursors (PN, NS, and PW) are presented in Table 2.

Micromeritics ASAP 2420 instrument was used for surface textural parameter measurements of the prepared ACs, by $N_2$ uptake of the ACs at 77 K. The ACs were degassed first at 120 °C temperature for 16 hours before Micromeritics measurements. The specific surface area ($S_{BET}$) was calculated by following the standard, Brunauer−Emmett−Teller (BET) method utilising the $N_2$ isotherm adsorption data within 0.01 to 0.1 relative pressure range. The adsorbed quantities of $N_2$ at $P/P_0$ of ca. 0.99 of ACs, were used for the calculation of total or cumulative pore volumes ($V_{total}$). Average pore diameter was determined using $4V_{total}/S_{BET}$ [24].

The volume of micropore ($V_{micro}$), was estimated by t-plot method, total mesopore volume $V_{meso}$ obtained by subtracting the micropore volume from the total pore volume [25]. Then the micro porosity percentage of the selected ACs was calculated by $V_{micro}/V_{total}$. Similarly, the mesoporosity percentage was calculated by using $V_{meso}/V_{total}$. Crystallographic analyses of the synthesised carbons before and after activation were inspected with the help of D8 Advance XRD diffractometer (Bruker Inc., Germany) and Cu Kα radiation source. While the value of voltage, the current used for the XRD experiments was 40 kV and 40 mA respectively.

Organic moieties generated on the surface of ACs were characterised by Fourier Transform Infrared (FTIR) Spectroscopy (Bruker Vertex 70 spectrometer) [26]. For FTIR investigations sample pellets were prepared with potassium bromide salt. The spectras were noted in between 400–4000 $cm^{-1}$ wave number range. The Mortar was used to ground 0.0015 g sample with 0.25 g of KBr. The obtained powder was then placed under a mechanical pressure of 10 $kPa/mm^2$ in a circular die, for 10 seconds. After this, the sample was transferred to an oven for drying at 100 $^oC$ for 48 hours under vacuum to avoid any interface between the mix, $CO_2$ molecules and water vapours. The temperature was reduced to room temperature under vacuum overnight. At the last, the sample was transferred to the analyser.

Surface morphology of all the raw samples, as well as the best performing ACs derived from these samples were obtained by using a scanning electron microscope (SEM) instrument JEOL 7100F FEG-SEM at 15 kV. Between three and four repeat runs for each experiment were made to ensure appropriate repeatability and validity of the results.

# 3 Results and discussion

Best performing ACs were screened from each group on the basis of their $CO_2$ uptake for further characterisation.

## 3.1 Evaluation of $CO_2$ capture performance

From TGA analyses, $CO_2$ adsorption (over $N_2$ balance) isotherms of the twelve fabricated ACs (Table 1) are plotted and reported in Fig. 1 to Fig. 3. Adsorption kinetics were estimated from TGA, as a function of time in the presence of 25 $^oC$ temperature. From these $CO_2$ adsorption isotherms, it is shown that the remarkable $CO_2$ uptake capacity of the ACs ranges from 2.53 to 3.92 mmol/g. While the lower range of $CO_2$ (over $N_2$ balance) uptake (2.53 mmol/g) of this study is comparable to other ACs synthesised from phenolic resins [27] and rice husk waste [4]. Phenolic resin based carbons were activated with different ratio of $HNO_3$ while rice husk carbons were activated with different KOH ratio. In both of these previous studies, $CO_2$ adsorption, at 25 $^oC$ temperature and 0.15 bar pressure, was not more than 2 mmol/g. Here in synthesised ACs derived from three different biomass precursors (NS, PN and PW). Each biomass sample/ or non-activated carbon was reacted with four different ratios of KOH, therefore, fabricated four different ACs i.e., NSK1, NSK2, NSK3 and NSK4 are the synthesised ACs from walnut shell biomass. Treatment with KOH changes the textural properties and chemical nature of functional groups of precursors. Activation with a different mass ratio of KOH strategy was applied in this study to prepare K-ACs with high porosity, surface area and increased amount of basic oxygen functionality, and all these factors helped in higher $CO_2$ uptake as verified from [28]. This strategy of activation of the carbons with different KOH ration was also proved to be beneficial from previous researches [28]. A higher amount of KOH helps in the generation of more porous structures followed by high $CO_2$ uptakes, this can be confirmed from Fig. 1, as different KOH amount yields different $CO_2$ uptake these results are in accordance with Singh, G., et al., [28].

As each biomass is intercalated with four different ratios of KOH, therefore, the $CO_2$ uptake values of 3.23>2.90>2.71>2.57 mmol/g were noted for walnut shell derived ACs NSK3>NSK4>NSK1>NSK2 respectively as shown in Fig. 1. These values are reported by rounding off the digits up to two decimal places. Similarly, 3.92>3.18>3.06>2.54 and 3.49>3.24>2.84>2.53 mmol/g uptake values were measured for KOH intercalated peanut shell and pine wood samples: PNK3>PNK1>PNK2>PNK4 (Fig. 2), and PWK1>PWK2>PWK3>PWK4 (Fig. 3) respectively. Best activated carbon from the walnut shell is NSK3, from peanut shell is PNK3 and from pine wood biomass is PWK1.

Comparatively, from these three groups, the most highly activated AC is PNK3 and least one is PWK4. In case of walnut shell ACs, 3.23 mmol/g of $CO_2$ adsorption peak value was noted, while the overall $CO_2$ adsorption is 60% in initial 4 minutes and after that, it was increased constantly with time for 1h. Similar trends were noted for other carbons in this time interval. Up to 16 minutes NSK4 showed a higher rate of uptake, but after that NSK3 exhibited a sudden increase in $CO_2$ uptake and goes on increasing up to 60 minutes. The $CO_2$ uptake capacity of different walnut shell ACs is different and increased little by increasing the mass ratio of KOH (in KOH/sample) up to 3:1, beyond this combination, further increase in the amount of activating agent did not increase the $CO_2$ uptake of the activated carbon (Fig. 1). For NSK4 the $CO_2$ uptake is lowered to some extent as compared to NSK3 that could be because of the lower number of adsorption, active and suitable functional group sites.

For peanut shell derived ACs, 3.92 mmol/g $CO_2$ adsorption peak value was noted, while the overall $CO_2$ adsorption is equivalent to 80% in initial 3 to 4 minutes. After this initial 80% adsorption capacity, horizontal plateaus of adsorption isotherms were observed for PNK1 and

PNK2, indicating the saturation of available microspores (Fig. 2). A constant increase of adsorption with time was observed for PNK3 also illustrates from its blue isotherm (Fig. 2). But for PNK4, a decrease in adsorption capacity was observed that was similar to NSK4 isotherm. Likewise, for pine wood derived ACs, the peak value of 3.49 mmol/g for $CO_2$ adsorption was observed. The overall $CO_2$ adsorption is equivalent to 91% in initial 2 to 3 minutes, again followed by somewhat horizontal plateaus of adsorption for PWK1 and PWK2 [4]. While for PWK3 and PWK4 relatively lower adsorptions were noted that could be because of a decrease in porosity with an increase in KOH activation, noted just for this group ACs (Fig. 3).

Physisorption carbons with porous surfaces have reasonably fast kinetics [29]; comprise diffusional transports in micro and macropores. That's why this study is designed on the physisorption principle ($CO_2$ uptake). All these $CO_2$ adsorption kinetics results, in association with a different mass ratio of KOH, concluded that the best group from these three which has shown fast $CO_2$ uptake rate is PW derived ACs, while the group which has shown higher $CO_2$ adsorption capacity is PN derived ACs (Fig. 4). The adsorption amounts reported with TGA are $CO_2$ adsorption over $N_2$ balance rather than pure $CO_2$ adsorption [4], because flue gas comprises of 15% $CO_2$ in $N_2$ [30]. It is observed that $CO_2$ adsorption capacities of ACs are higher than $N_2$ but $N_2$ adsorbs little with $CO_2$ in flue gas analysis. While the amount of $N_2$ is reported usually less or equals to 0.5 mmol/g [31].

## 3.2 Textural analysis of activated carbons

$N_2$ adsorptions were performed for six samples (Fig. 5) from twelve, among which three were those exhibited higher $CO_2$ uptake (PNK3>PWK1>NSK3), and the other three selected ACs were those, either the least adsorbed carbon (PNK4) from a particular group of ACs with higher KOH ratio or the carbon with relatively higher $CO_2$ uptake but with least ratio of KOH (NSK1) from another group of ACs. The effect of this porosity on the adsorption of $N_2$ is shown in the form of $N_2$ adsorption isotherms. Surface textural and pore structure calculations obtained from the BET measurements are incorporated in Table 3. It can be seen that the $V_{total}$ and $S_{BET}$ increased from 0.07 to 0.38 $cm^3/g$ and 112.33 to 944.05 $m^2/g$ respectively, for different ACs fabricated at 750 $^oC$ and 0.15 bar pressure. It is cleared that the ACs derived from the protocol of KOH activation are microporous with the microporosity accounting for up to 95% of the total porosity.

The $N_2$ sorption (adsorption and desorption) isotherms of PNK3, PWK1, PNK4, NSK1 and PWK2 are found similar to Type I isotherm, which is also verified from the International Union of Pure and Applied Chemistry (IUPAC) data sources [32]. While one of the selected samples, NSK3 has shown Type II isotherm. Literature confirms that $N_2$ sorption Type I isotherms are obtained for adsorbents, those having very small pores usually known as micropores. The presence of these micropores verifies from the sharp $N_2$ uptake capacity of PNK3, PWK1, PWK2 and NSK1 adsorbents at low pressure <0.1. Afterwards, the development of horizontal plateaus at higher pressures attributed to an extraordinary microporosity of these four selected ACs ranges from 72 to 95%. These results provide the reasons for higher $CO_2$ uptake and fast adsorption kinetics of the above mentioned ACs.  At comparatively further higher pressures, variable minor to significant hysteresis loops are observed for PWK1, NSK3, PNK4, PWK2 and NSK1 ACs. Hysteresis loop suggests the presence of mesoporous surface of adsorbent at these pressures generated by the gas condensation  [22]. While Type II $N_2$ adsorption isotherm shown by the adsorbent, NSK3, indicates mesoporous surface with 15% microporosity.

Higher specific surface area and micropores volume of PNK3 and higher adsorption capacities of NSK3 and PWK1 derived ACs, support that the strategy of a variable amount of KOH used for activation from minor (1:1) to significant (1:4) range is successful. Increase in micropore volume and surface area is detected because of oxidation and gasification reactions proceed via decomposition of potassium carbonate ($K_2CO_3$) at a high temperature, is also supported with SEM images.

The lower $S_{BET}$ of two selected ACs; NSK3>PNK4, is 146.86>112.33 $m^2$/g. This decreasing order of $S_{BET}$, is observed with an increasing ratio of the activating agent in the synthesised ACs from (1:3 to 1:4). This might be because of the over oxidation of carbons and development of insoluble potassium (K) residues. The relatively lower $S_{BET}$ obtained for the activated carbons was because of K impregnation, which led to fractional or even thorough occlusion of pores. Therefore, a peak concentration of potassium is observed, above that the additional residual potassium (PNK4) helps little to capture $CO_2$. This discussion confirms that the overall best ratio among all the 12 fabricated ACs, derived from three different groups of precursors is 1:3 (sample: KOH) because on further activation with KOH leads to over oxidation and formed macro-pores credited to adsorption of 2.54 mmol/g of $CO_2$ uptake. From Table 3, it could be verified that the BET measurements for these adsorbents are consistent with their Type I (Fig. 5f) and Type II (Fig. 5e) isotherms [33]. Fig. S1 shows an observed comparative analysis of $N_2$ adsorbed volumes of the selected ACs, it is seen that the volume of $N_2$-adsorbed for PNK4 is very small owing to its relatively lower developed total pores $Vt_{otal}$.

The presence of different sizes of pores in selected ACs from each group is comparatively illustrated from Fig. 6. In the case of PNK3, PWK1 and PWK2, three different sizes of pores have been generated, micropores/mesopores (< 50 nm) and macropores (> 50 nm). While in the case of NSK1, NSK3 and PNK4 the most probably generated pores are < 50 nm in size. Among them, more are mesopores (2–50 nm) while some are micropores (< 2 nm). Fig. S2 investigates the bimodal pore structure and its development by KOH activation of best performing ACs from different groups. Fig. S3 shows an observed dependence of $CO_2$ uptake on the developed pore volume by KOH treatment.

## 3.3 KOH intercalation mechanism

Type I isotherms Fig. 5(a-d, f) are observed because of impregnation of KOH, acts as a catalyst to speed up the gasification reaction as mentioned in equations (2, 3, 5 and 6) [32, 34]. Reaction intermediates, $K_2CO_3$ and $K_2O$ are formed at a temperature >700 $^oC$. These polar/basic intermediates react with the carbon matrix to fabricate a framework with micropores. The carbon framework development from non-porous to porous upon treatment with KOH is confirmed by SEM analyses of ACs.

Polymeric components present in biomass undergo different chemical reactions including cracking, aromatisation, dehydration, dehydrogenation and depolymerisation, during the carbonisation process followed by treatment with KOH base [28]. The later reaction is applied to activate the carbon matrix through a series of reactions (1 to 8). The redox reaction of biomass carbon with KOH leads to oxidation of carbon matrix that yields potassium carbonate ($K_2CO_3$) and hydrogen ($H_2$) gas (reactions 2 to 4). The oxidation process and resultantly the presence of oxidised species on the surface of ACs are in agreement with relevant FTIR peaks in the developed oxidised functional group region (1000–1860 $cm^{-1}$).

$$2KOH \rightarrow K_2O + H_2O \quad (1)$$

$$C + H_2O \rightarrow CO + H_2 \quad (2)$$

$$CO + H_2O \rightarrow CO_2 + H_2 \quad (3)$$

$$CO_2 + K_2O \rightarrow K_2CO_3 \quad (4)$$

$$K_2CO_3 \rightarrow K_2O + CO_2 \quad (5)$$

$$CO_2 + C \rightarrow 2CO \quad (6)$$

$$C + K_2O \rightarrow C\text{-}O\text{-}K + K \quad (7)$$

$$C + K_2O \rightarrow 2K + CO \quad (8)$$

Progressively, as the temperature arose the chemicals/functional groups of biomass decompose and gasification occurs (reactions 5, 6 and 8), the rest of the mass forms char through aromatisation reaction. The presence of aromatic groups after activation is observed from the FTIR peaks of activated carbons in the related fingerprint region of (808–893 $cm^{-1}$). Gasification/ or escape of volatile components cause the development of porous surface from non-porous carbon framework/matrix [20].

The biomass carbon reacts with the KOH until it is consumed completely and as a result converted into metallic K, and other volatiles. $K_2CO_3$ formed, further reacts with carbon (biomass) to generate $K_2O$, K and volatiles (reactions 4 to 8). The development of high porosity is credited to the (reactions 2 to 8) of dehydration, polymerisation and evolution of gases. Potassium based compounds formed (reaction 7) during the activation process are well intercalated/ or impregnated into the carbon framework. While later the removal of these compounds (K species) using water treatment results in the fabrication of porous surfaces of ACs [32]. Therefore, it can be said that the possible effect of the KOH treatment on the studied carbons was porosity generation with the well observed gasification reactions.

## 3.4 Crystalline surface analysis

The synthesised $CO_2$ adsorbents have been studied for their microcrystalline or amorphous nature by powdered XRD patterns (Fig. 7). These analyses were applied to a selected number of activated (NSK1, NSK3, PNK3, PNK4, PWK1 and PWK2) and corresponding non-activated (NS, PN and PW) carbons, to identify the changes on the surface of the adsorbents before and after activation. The peak intensities in case of activated carbons and non-activated carbons are in exact accordance with the KOH ratio. In case of all non-activated and some activated carbons, one broad and two weak peaks have been noted around $2\theta = 22–25^{o}$, $43^{o}$ and $45^{o}$. A broad peak of quite high intensity around $22–25^{o}$ is observed, for NS, PN and PW carbons, and confirms the amorphous nature of non-activated carbons. This peak around $22–25^{o}$ is identical to (002) diffraction of graphite and confirms the hexagonal nature of NS, PN and PW carbons. While the two weak peaks around $2\theta = 43^{o}$ and $45^{o}$ corresponded to the (101) and (100) diffraction planes of graphite are observed in relation to their partial microcrystalline nature [4].

A clear shift in XRD peaks has been observed for activated carbons in comparison to non-activated carbons of all groups. In case of walnut shell derived activated carbon, NSK1, relatively less intense peaks are detected around $25^{o}$, $43^{o}$ and $45^{o}$. The peak of (002) diffraction plane of graphite is absent in case of NSK3 in comparison to raw non-activated carbon NS, and the absence of this characteristic peak might be because of the collapse of the carbon matrix. The encircled area sharp peaks of NSK3 may be attributed to the development of more chemical species in the interlayers of collapse hexagonal graphite (carbon). Likewise, in case of peanut shell derived ACs, again interesting surface chemistry has been confirmed from XRD patterns. Broad peaks around the characteristic range of $22–25^{o}$ and $43^{o}$ in case of non-activated PN are developed into sharp ones for PNK3, as because of increasing KOH ratio. As it is observed from XRD pattern that sample/KOH ratio of 1:4 is not helpful in the activation of carbons, because, in case of PNK4, almost peaks disappeared in comparison to PNK3 and PN. The intensity of the observed peaks is also lowered in comparison to 1:3 and 1:2 ratio. This type of behaviour might be noted as of destructive interferences develop because of a relatively high amount of KOH [20]. This destructive interference of the KOH might cause the degradation of the porous structures. XRD profiles of pine wood groups are exactly similar to the peanut shell group. The peak centred around 26° to 27° is noted for the generation of inorganic crystalline compounds [35].

## 3.5 Surface chemistry analysis

FTIR analyses were performed for six samples. Three were non-activated carbons: NS, PN and PW and three ACs: NSK3, PNK3 and PWK1. In case of walnut shell based, non-activated carbon NS; the presence of peaks at 3664 (O-H str), 3263 (N-H str), 2467 (O-H str), 1857 (C=O str), 1660 (C=O str), 1463, 1326 (O-H def) and 690 (CH def) $cm^{-1}$ correspond to OH, NH or might be chelate, carboxylic acid, carbonyl group of quinone, α-β unsaturated ketone, methyl, alcohol and alkenyl groups (Fig. 8). While this precursor on activation with KOH in 1:3 ratio yield NSK3, which on analysis gave spectra that confirms its activation and graphitisation as well, similar results are obtained from XRD profiles of these materials. The peaks of NSK3 at 3664 (O-H str), 3263 (N-H str), 2397, 1774 (C=O str), 1620 (C=O str), 1458 (C=C), 1344 (O-H def), 1120 (C-O str), 808 (CH def) and 617 (CH def) $cm^{-1}$ indicate the generation of OH, NH/ or might be chelate, carboxylic acid, ester, carbonyl group with benzene, double bond of the aromatic ring, alcohol, ether, *p*-substituted aromatic ring and alkenyl groups (Fig. 8). Like NSK3, almost similar type of functional groups were developed on the surface of PNK3 after activation, might be because of the same mass ratio of the activating agent.

The presence of peaks at 3691 (O-H str), 2891 (CH str), 2380, 1832 (C=O), 1645 (C=O str), 1450 (def), 1249 (C-O str) and 640 (def) $cm^{-1}$ correspond to OH, aldehyde, carboxylic acid, carbonyl of anhydride, carbonyl of diaryl ketone, methyl, diaryl ether and CH groups in case of PN non-activated carbon (Fig. 9). This precursor on activation with KOH in 1:3 ratio fabricated PNK3, which on FTIR analysis gave spectra, that confirms its activation, furthermore, these FTIR results are also supported with SEM results of the respective AC. The peaks of PNK3 at 3514 (O-H str), 2437, 1853 (C=O str), 1714 (C=O str), 1575 (N-H def), 1398 (O-H def), 1002 (C-O str), 873 (CH def) and 723 (rocking *v*) $cm^{-1}$ correspond to dimer or chelate, carboxylic acid, carbonyl of anhydride, carbonyl of diaryl ketone, aromatic amine, phenol, ether, substituted aromatic ring and CH groups (Fig. 9).

Likewise, for PW precursor the bands at 2314, 1799 (C=O str), 1672 (C=O str), 1471 (def) and 779 (CH def) $cm^{-1}$ correspond to carboxylic acid, carbonyl of acid halide, carbonyl of diaryl ketone, CH3, *m*-disubstituted aromatic group, while PWK1 with 1:1 KOH/sample ratio indicated bands at 3683 (O-H str), 2351, 2250 (str), 1814 (C=O), 1635 (N-H def), 1469, 1315 (C-O),1112 (C-O str), 893, 798 and 657 $cm^{-1}$ attribute to free OH, carboxylic acid, alkenyl, carbonyl of acid halide, secondary amine, alcohol, C-O of anhydride, ether, two bands for weak and strong *m*-disubstituted aromatic ring and CH groups (Fig. 10). The presence of dimers, chelates and disubstituted aromatic ring in case of PNK3, NSK3 and PWK1, confirms the aromatisation reactions with KOH impregnation. The developed basic groups of ACs help in the adsorption of acidic $CO_2$ because of electrostatic interactions developed between them at a higher temperature (reaction 7).

## 3.6 Surface morphology analysis

The morphological analyses were carried out for non-activated (NS, PN and PW) precursors and the best performed ACs include; NSK3 from NS, PNK3 from PN and PWK1 from PW. These ACs not only showed higher $CO_2$ uptake in their groups but also confirmed with FTIR spectra, the modified surface chemistries in comparison to their non-activated forms as a result of activation. Walnut shell based non-activated precursors, NS shows non-porous and flat morphology, in comparison to their activated form NSK3 as illustrated in (Fig. 11). SEM images of NSK3, clearly shows changed surface morphology than precursor not showing more microspores. Additionally, the pore diameter of NSK3 is seen much larger than other porous ACs; PNK3 (Fig. 12d) and PWK1 (Fig. 13b).

Moreover, it could reasonably be said that the decomposition of carbon matrix/walls of NSK3 connecting porous structure via a high content of KOH took place. Carbon walls oxidised at high temperature 750 $^{o}$C, generated K residues, those changing its morphology completely. Therefore, it could be concluded that NSK3, revealed a carbon matrix collapse with a higher mass ratio of KOH. Sometimes, if the higher $CO_2$ capture of activated carbons (K-ACs) cannot be compatible with surface textural features, porosity decreases with activation. Then in such cases, the higher $CO_2$ uptake of K-ACs attributes to modified surface chemistries [28]. In the case of NSK3, potassium intercalation, instead of relatively lower microporosity plays a key role in the $CO_2$ capacities. Therefore, it could be said that the polarized surface functional groups are helpful to enhance surface interaction with the quadrupole moment of $CO_2$ and consequently instigated higher $CO_2$ uptake [28].

The SEM images of non-activated peanut shell derived precursor, PN, showed a flat non-porous surface and developed into a highly porous surface (PNK3) on treatment with an activating agent as illustrated in Fig. 12. Removal of gases during the process of activation according to the redox stoichiometric equations (5–6, 8) were credited to the flat, regular and 87% microporosity of PNK3 [20]. These pores justify the more diffusion/ or adsorption of $CO_2$ from bulk to the adsorbent, PNK3 surface. Porosity generation phenomenon was also observed similar to peanut shell in pine wood group. There is a clear difference between the morphological surfaces of PW, PWK1, non-activated and activated forms of pine wood precursor and carbon respectively as shown in Fig. 13.

## 3.7 Fast adsorption potential

$CO_2$ adsorption (over $N_2$ balance) measurements for the first 120 seconds have been reported for activated carbons. The measurement of the $CO_2$ uptake of the adsorbents in the first 120 seconds in comparison to 1 hour verified that the developed ACs are very responsive and free from time dependent factor to much extent. From Table 4, it could be observed that almost all adsorbents with one or two exceptions showed an average of more than 60% uptake of $CO_2$ from total in the first 120 seconds. In the case of walnut shell derived ACs (Fig. S4(a)) the $CO_2$ uptake in first 120 sec is 50% in average, which is 20% lower than peanut shell derived ACs (Fig. S4(b)) and 30% lower than pine wood derived ACs (Fig. S4(c)). The possible reason behind this could be the different composition and diverse nature of the material. Moreover, PNK2 and PWK2 have presented an ideal case by adsorbing more than 90% of $CO_2$ from the total in the first 120 seconds. Under the current scenario of environmental pollution [36, 37], there is a need to develop renewable fuels [38] and sustainable technologies [39, 40] to reduce $CO_2$ emissions and control global warming [41]. Hence, biomass based carbon adsorbents are excellent renewable materials that could be used to capture $CO_2$ from coal fired power plants.

## 3.8 Cost estimation

From cost estimation analysis with respect to per kg production, it is observed that the herein synthesised ACs are cheaper and comparable to the other commercially available ones. An amount of 1.93 US$ is calculated for the production of per kg of AC of this study as shown in Table 5, while the amount of commercially available AC is in the range of 2 to 5 US$ per kg [42]. In literature, the synthesised ACs from the peels of *Artocarpus integer* fruit following the steam activation method were estimated to be cost-effective adsorbents (1.67 US$ per kg) [42], but these carbons were not evaluated for their $CO_2$ uptake potentials. Furthermore, the cost estimation analysis was carried out by following the summation of sample per kg cost of different components [42].

# 4 Conclusions

Detailed screening and development of adsorbents/ACs from diverse biomass residues, which are cheap, low cost, sustainable, green agricultural waste, easily available and $CO_2$ neutral materials is carried out. This synthesis of ACs from biomass precursors will not only overcome the global warming issue but would also minimise the problems of land space covered by the selected biomass residues.

- TGA and BET analyses demonstrate that the adsorption capacities of different ACs are; 3.23>2.90>2.71>2.57, 3.92>3.18>3.06>2.54 and 3.49>3.24>2.84>2.53 mmol/g noted for NSK3>NSK4>NSK1>NSK2, PNK3>PNK1>PNK2>PNK4 and PWK1>PWK2>PWK3>PWK4 respectively, among all these the highest $CO_2$ (3.92 mmol/g) is noted with PNK3 AC that is peanut shell derived.
- $N_2$ adsorption isotherms show Type I isotherm for NSK1, PNK3, PNK4, PWK1 and PWK2 and Type II isotherm for NSK3.
- Bimodal pore structure analyses verify the Type I and Type II $N_2$ sorption isotherms results.
- Peaks in the region < 50 nm, confirm that mostly the adsorbents' surface comprised of micro and mesopores.
- The catalytic KOH mechanistic approach and the resultant aromatization and gasification reactions are in accordance with FTIR peaks in (808–893 $cm^{-1}$) region and verified from SEM images.

- Characteristic XRD peaks of 2θ = 22-25$^o$ and 43$^o$ in case of non-activated precursors are developed into sharp ones for ACs.
- Cost estimation calculation showed that the developed ACs are cheaper in comparison to commercially available ones.
- Future research could be directed towards soft woody biomass residues because they yield relatively more porous adsorbents upon activation with KOH than hard woody biomass.

## Acknowledgement

The authors are thankful to the Higher Education Commission of Pakistan for the financial support to carry on this research.

# References


1. Li, J., et al., Selective preparation of biomass-derived porous carbon with controllable pore sizes toward highly efficient CO2 capture. Chemical Engineering Journal, 2019. 360: p. 250-259.
2. Sher, F., et al., Thermal and kinetic analysis of diverse biomass fuels under different reaction environment: A way forward to renewable energy sources. Energy Conversion and Management, 2020. 203: p. 112266.
3. Li, B., et al., Advances in CO2 capture technology: A patent review. Applied Energy, 2013. 102: p. 1439-1447.
4. Liu, X., et al., Potassium and zeolitic structure modified ultra-microporous adsorbent materials from a renewable feedstock with favorable surface chemistry for co2 capture. ACS applied materials & interfaces, 2017. 9(32): p. 26826-26839.
5. Sher, F., et al., Oxy-fuel combustion study of biomass fuels in a 20 kW th fluidized bed combustor. Fuel, 2018. 215: p. 778-786.
6. Sher, F., et al., Experimental investigation of woody and non-woody biomass combustion in a bubbling fluidised bed combustor focusing on gaseous emissions and temperature profiles. Energy, 2017. 141: p. 2069-2080.
7. Hai, I.U., et al., Experimental investigation of tar arresting techniques and their evaluation for product syngas cleaning from bubbling fluidized bed gasifier. 2019. 240: p. 118239.
8. Figueroa, J.D., et al., Advances in $CO_2$ capture technology—The US Department of Energy's Carbon Sequestration Program. International Journal of Greenhouse Gas Control, 2008. 2(1): p. 9-20.
9. Coninck, H.d., et al., IPCC special report on carbon dioxide capture and storage. Intergovernmental Panel on Climate Change, 2005.
10. Wang, M., et al., Post-combustion CO2 capture with chemical absorption: a state-of-the-art review. Chemical Engineering Research and Design, 2011. 89(9): p. 1609-1624.
11. Hai, I.U., et al., Assessment of biomass energy potential for SRC willow woodchips in a pilot scale bubbling fluidized bed gasifier. 2019. 258: p. 116143.
12. Ao, W., et al., Microwave assisted preparation of activated carbon from biomass: A review. Renewable and Sustainable Energy Reviews, 2018. 92: p. 958-979.
13. Djilani, C., et al., Adsorption of dyes on activated carbon prepared from apricot stones and commercial activated carbon. Journal of the Taiwan Institute of Chemical Engineers, 2015. 53: p. 112-121.
14. Hazzaa, R. and M. Hussein, Adsorption of cationic dye from aqueous solution onto activated carbon prepared from olive stones. Environmental Technology & Innovation, 2015. 4: p. 36-51.
15. Nowicki, P., J. Kazmierczak, and R. Pietrzak, Comparison of physicochemical and sorption properties of activated carbons prepared by physical and chemical activation of cherry stones. Powder Technology, 2015. 269: p. 312-319.
16. Jimenez-Cordero, D., et al., Preparation of granular activated carbons from grape seeds by cycles of liquid phase oxidation and thermal desorption. Fuel Processing Technology, 2014. 118: p. 148-155.
17. Ello, A.S., et al., Coconut shell-based microporous carbons for CO2 capture. Microporous and Mesoporous Materials, 2013. 180: p. 280-283.
18. Tay, T., S. Ucar, and S. Karagöz, Preparation and characterization of activated carbon from waste biomass. Journal of Hazardous Materials, 2009. 165(1-3): p. 481-485.

19. Wahby, A., et al., High-surface-area carbon molecular sieves for selective CO2 adsorption. ChemSusChem, 2010. 3(8): p. 974-981.
20. Tiwari, D., H. Bhunia, and P.K. Bajpai, Adsorption of CO2 on KOH activated, N-enriched carbon derived from urea formaldehyde resin: kinetics, isotherm and thermodynamic studies. Applied Surface Science, 2018. 439: p. 760-771.
21. Jiang, L., et al., Post-combustion CO2 capture from a natural gas combined cycle power plant using activated carbon adsorption. Applied Energy, 2019. 245: p. 1-15.
22. Liu, J., et al., Spherical potassium intercalated activated carbon beads for pulverised fuel CO2 post-combustion capture. Carbon, 2015. 94: p. 243-255.
23. Sait, H.H., et al., Pyrolysis and combustion kinetics of date palm biomass using thermogravimetric analysis. Bioresource Technology, 2012. 118: p. 382-389.
24. Lin, G., et al., KOH activation of biomass-derived nitrogen-doped carbons for supercapacitor and electrocatalytic oxygen reduction. Electrochimica Acta, 2018. 261: p. 49-57.
25. Hirst, E., A. Taylor, and R. Mokaya, A simple flash carbonization route for conversion of biomass to porous carbons with high CO2 storage capacity. Journal of Materials Chemistry A, 2018.
26. Yakout, S. and G.S. El-Deen, Characterization of activated carbon prepared by phosphoric acid activation of olive stones. Arabian Journal of Chemistry, 2016. 9: p. S1155-S1162.
27. Sun, N., et al., Surface-modified spherical activated carbon materials for pre-combustion carbon dioxide capture. RSC Advances, 2015. 5(42): p. 33681-33690.
28. Singh, G., et al., Single step synthesis of activated bio-carbons with a high surface area and their excellent CO2 adsorption capacity. Carbon, 2017. 116: p. 448-455.
29. Presser, V., et al., Effect of pore size on carbon dioxide sorption by carbide derived carbon. Energy & Environmental Science, 2011. 4(8): p. 3059-3066.
30. Rashidi, N.A. and S. Yusup, An overview of activated carbons utilization for the post-combustion carbon dioxide capture. Journal of CO2 utilization, 2016. 13: p. 1-16.
31. Li, M. and R. Xiao, Preparation of a dual pore structure activated carbon from rice husk char as an adsorbent for CO2 capture. Fuel processing technology, 2019. 186: p. 35-39.
32. Liu, X., et al., Developing hierarchically ultra-micro/mesoporous biocarbons for highly selective carbon dioxide adsorption. Chemical Engineering Journal, 2019. 361: p. 199-208.
33. Güleç, F., F. Sher, and A. Karaduman, Catalytic performance of Cu-and Zr-modified beta zeolite catalysts in the methylation of 2-methylnaphthalene. Petroleum Science, 2019. 16(1): p. 161-172.
34. Wang, J. and S. Kaskel, KOH activation of carbon-based materials for energy storage. Journal of Materials Chemistry, 2012. 22(45): p. 23710-23725.
35. Wang, K., et al., Promising biomass-based activated carbons derived from willow catkins for high performance supercapacitors. Electrochimica Acta, 2015. 166: p. 1-11.
36. Cuce, E., et al., Strategies for ideal indoor environments towards low/zero carbon buildings through a biomimetic approach. International Journal of Ambient Energy, 2019. 40(1): p. 86-95.
37. Zhang, Y., et al., Simulation of Particle Mixing and Separation in Multi-Component Fluidized Bed Using Eulerian-Eulerian Method: A Review. International Journal of Chemical Reactor Engineering, 2019. 17(11).
38. Al-Juboori, O., et al., The effect of variable operating parameters for hydrocarbon fuel formation from CO2 by molten salts electrolysis. Journal of CO2 Utilization, 2020. 40: p. 101193.

39. Al-Shara, N.K., et al., Electrochemical study of different membrane materials for the fabrication of stable, reproducible and reusable reference electrode. Journal of Energy Chemistry, 2020. 49: p. 33-41.
40. Cuce, E., et al., Sustainable ventilation strategies in buildings: CFD research. Sustainable Energy Technologies and Assessments, 2019. 36: p. 100540.
41. Hassan, M.H.A., et al., Kinetic and thermodynamic evaluation of effective combined promoters for CO2 hydrate formation. Journal of Natural Gas Science and Engineering, 2020: p. 103313.
42. Selvaraju, G. and N.K.A. Bakar, Production of a new industrially viable green-activated carbon from Artocarpus integer fruit processing waste and evaluation of its chemical, morphological and adsorption properties. Journal of cleaner production, 2017. 141: p. 989-999.

# List of Tables

**Table 1.** Newly synthesised green activated carbons (ACs) with different ratio of the activating agent with raw material.

| Sample ID | Composition (m/m) | Mass ratio (sample: KOH) | Chemical activation temperature (ºC) |
|---|---|---|---|
| [a]NSK1 | Walnut shell + potassium | 1:1 | 750 |
| [a]NSK2 | Walnut shell + potassium | 1:2 | 750 |
| [a]NSK3 | Walnut shell + potassium | 1:3 | 750 |
| [a]NSK4 | Walnut shell + potassium | 1:4 | 750 |
| [b]PNK1 | Peanut shell + potassium | 1:1 | 750 |
| [b]PNK2 | Peanut shell + potassium | 1:2 | 750 |
| [b]PNK3 | Peanut shell + potassium | 1:3 | 750 |
| [b]PNK4 | Peanut shell + potassium | 1:4 | 750 |
| [c]PWK1 | Pine wood + potassium | 1:1 | 750 |
| [c]PWK2 | Pine wood + potassium | 1:2 | 750 |
| [c]PWK3 | Pine wood + potassium | 1:3 | 750 |
| [c]PWK4 | Pine wood + potassium | 1:4 | 750 |

*** Note: [a]NSK1, walnut shell sample activated with potassium in different m/m ratio; [b]PNK1, Peanut shell sample activated with potassium in different m/m ratio; [c]PWK1, Pine wood sample activated with potassium in different m/m ratio.

**Table 2.** Chemical analyses of biomass samples.

| **Biomass samples** | **Ultimate analysis**[a] | | | | | | | **Proximate analysis**[c] | | | |
|---|---|---|---|---|---|---|---|---|---|---|---|
| | C (%) | H (%) | N (%) | O[b] (%) | S (%) | H/C | O/C | M (%) | VM (%) | FC (%) | Ash (%) |
| Walnut shell | 45.67 | 6.27 | 0.40 | 47.39 | 0.28 | 0.14 | 1.04 | 7.66 | 68.56 | 21.96 | 1.82 |
| Peanut shell | 46.34 | 6.42 | 1.95 | 45.07 | 0.23 | 0.14 | 0.97 | 6.45 | 71.87 | 17.50 | 4.18 |
| Pine wood | 44.78 | 6.17 | 0.42 | 48.38 | 0.26 | 0.14 | 1.08 | 6.97 | 72.54 | 17.07 | 3.47 |

M, VM, and FC value on dry basis except as denoted in the table.

a. Calculated by the difference.
b. On dry basis except moisture which is on as received basis.
c. As received basis.

**Table 3.** Surface and pore structure statistics of ACs measured from $N_2$ sorption.

| **Sample** | $S_{BET}$ ($m^2$/g) | $V_{total}$ ($cm^3$/g) | **Average pore diameter** (nm) | $V_{micro}$ ($cm^3$/g) | $V_{meso} = V_{total} - V_{micro}$ ($cm^3$/g) | **Microporosity** $= V_{micro}/V_{total}$ (%) | **Mesoporosity** $= V_{meso}/V_{total}$ (%) |
|---|---|---|---|---|---|---|---|
| PNK3 | 900.76 | 0.38 | 1.69 | 0.33 | 0.05 | 87 | 13 |
| PNK4 | 112.33 | 0.07 | 2.49 | 0.04 | 0.03 | 57 | 43 |
| NSK1 | 603.25 | 0.22 | 1.46 | 0.21 | 0.01 | 95 | 5 |
| NSK3 | 146.86 | 0.26 | 7.08 | 0.04 | 0.22 | 15 | 85 |
| PWK1 | 944.05 | 0.35 | 1.48 | 0.33 | 0.02 | 94 | 6 |
| PWK2 | 581.07 | 0.29 | 1.99 | 0.21 | 0.08 | 72 | 28 |

**Table 4.** $CO_2$ uptake rate of synthesised adsorbents.

| ACs | Uptake in 1 hour | Uptake in first 120 sec | % $CO_2$ uptake in first 120 sec |
|---|---|---|---|
| NSK1 | 2.71 | 1.55 | 57.30 |
| NSK2 | 2.57 | 1.35 | 52.67 |
| NSK3 | 3.23 | 1.34 | 41.64 |
| NSK4 | 2.90 | 1.48 | 50.91 |
| PNK1 | 3.18 | 2.80 | 88.05 |
| PNK2 | 3.06 | 2.77 | 90.38 |
| PNK3 | 3.92 | 2.38 | 60.76 |
| PNK4 | 2.54 | 1.04 | 41.11 |
| PWK1 | 3.49 | 3.01 | 86.21 |
| PWK2 | 3.24 | 3.06 | 94.49 |
| PWK3 | 2.84 | 2.00 | 70.49 |
| PWK4 | 2.53 | 1.76 | 69.66 |

** $CO_2$ adsorption (over $N_2$ balance)

**Table 5**. Estimated cost production of ACs via KOH activation (US$/ kg).

| Components | US$/ kg |
|---|---|
| KOH | 0.38 |
| Distilled water | 0.50 |
| Nitrogen gas | 0.20 |
| Power consumption | 0.80 |
| Transportation | 0.05 |
| Total | 1.93 |

# List of Figures

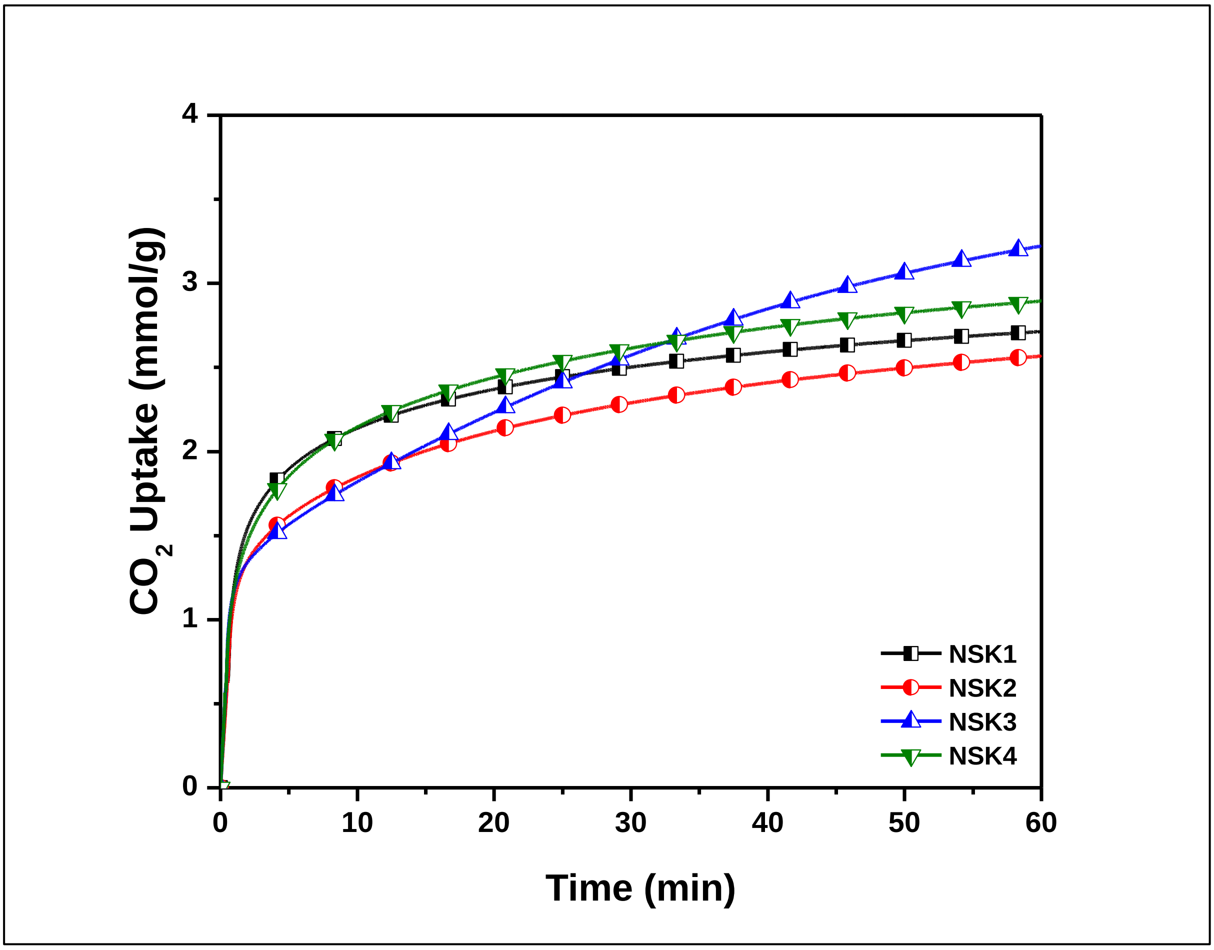


**Fig. 1.** $CO_2$ uptake isotherms of walnut shell derived ACs at 25 °C.

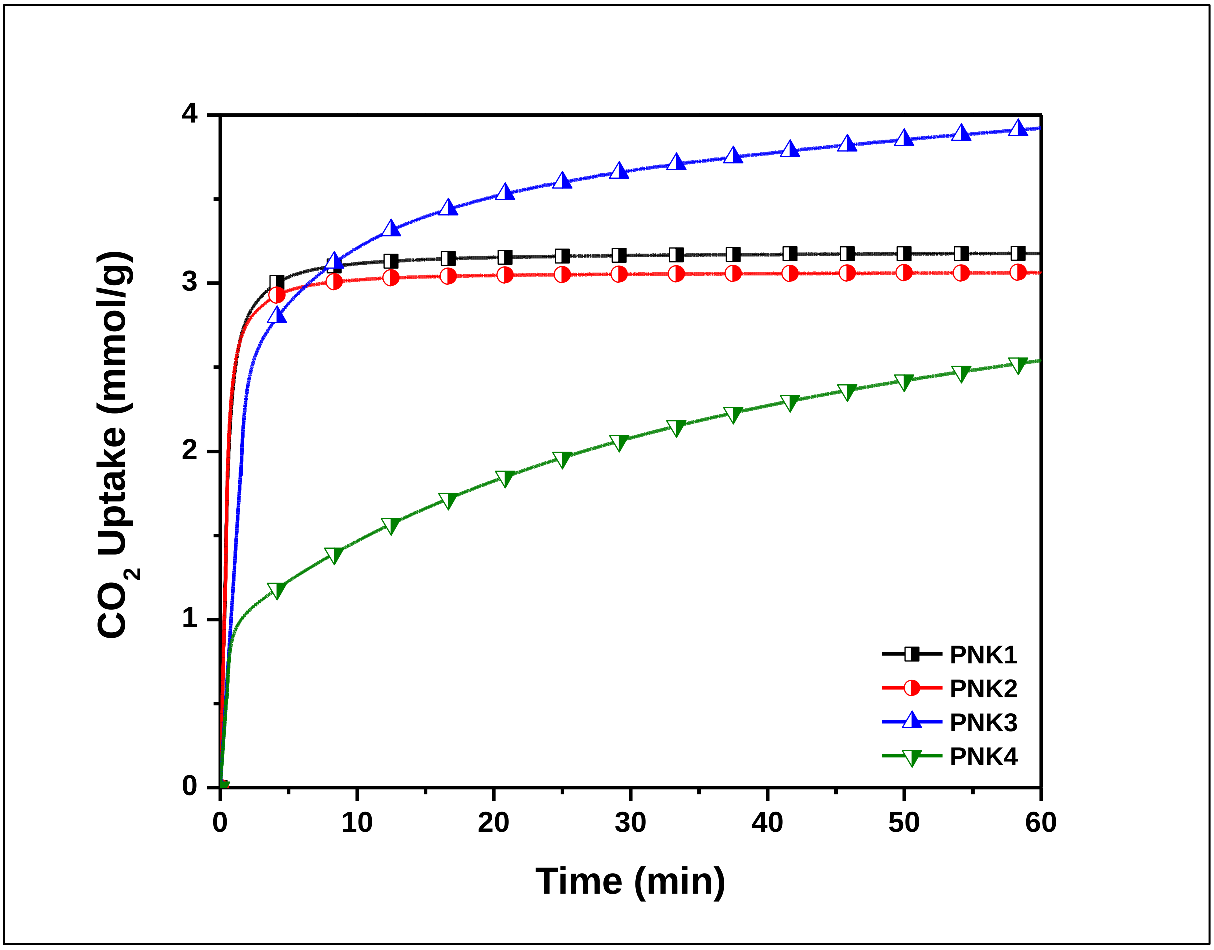


**Fig. 2.** $CO_2$ uptake isotherms of peanut shell derived ACs at 25 °C.

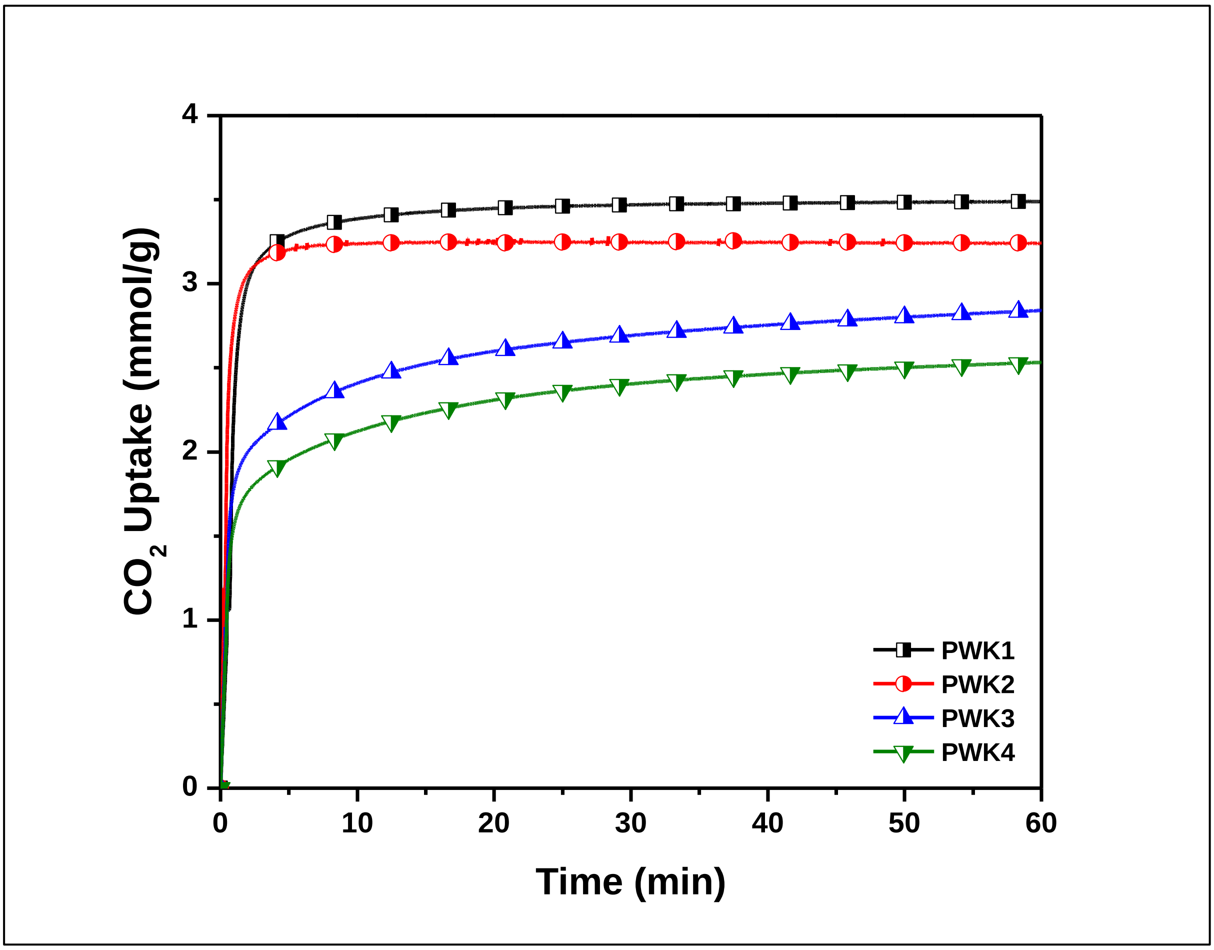


**Fig. 3.** $CO_2$ uptake isotherms of pine wood derived ACs at 25 °C.

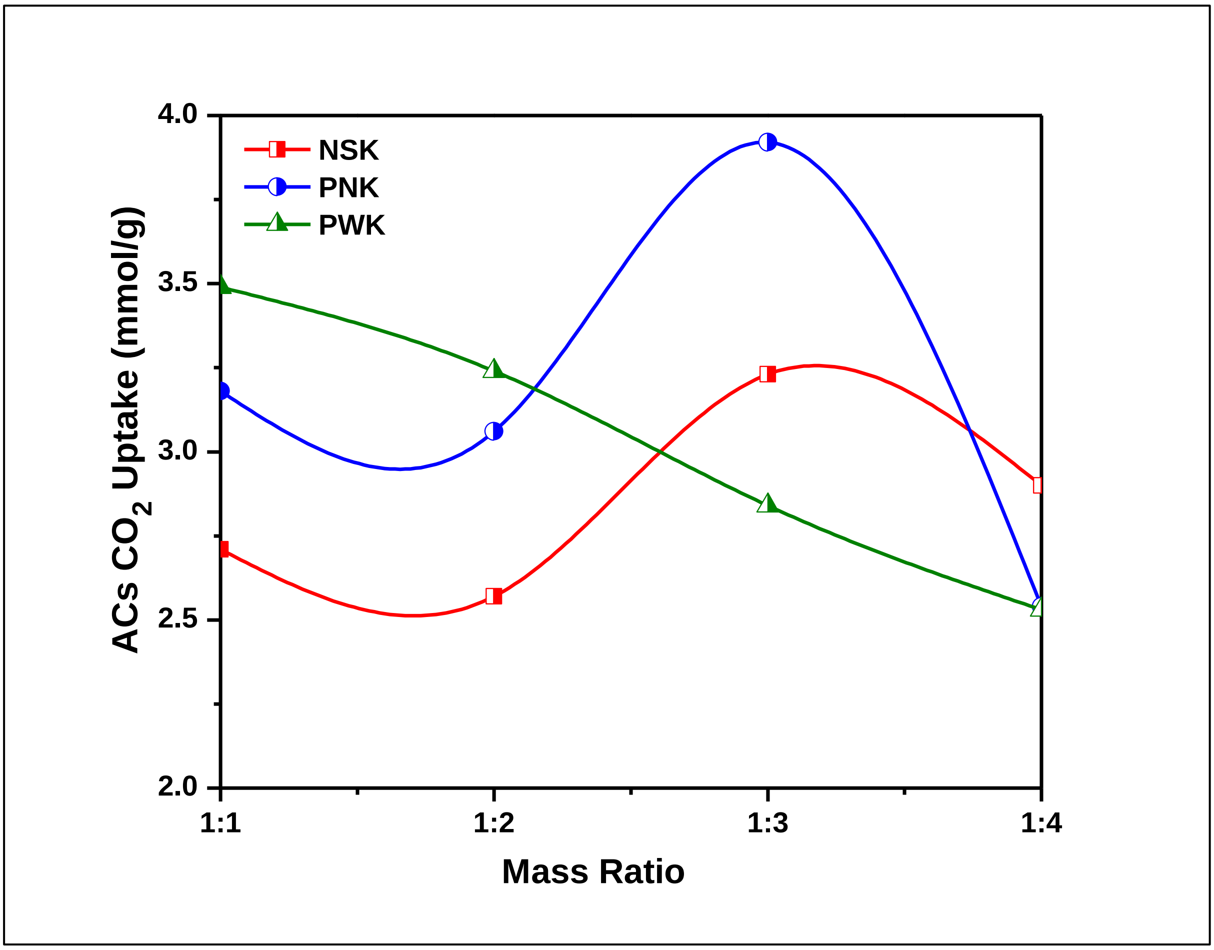


**Fig. 4.** The role of KOH in $CO_2$ uptake for adsorbents synthesised from different precursors.

**Note:** All Fig. 5 (a-f) will be combined into one figure under one caption. The authors have separated these figures just for a better understanding of the reviewers.

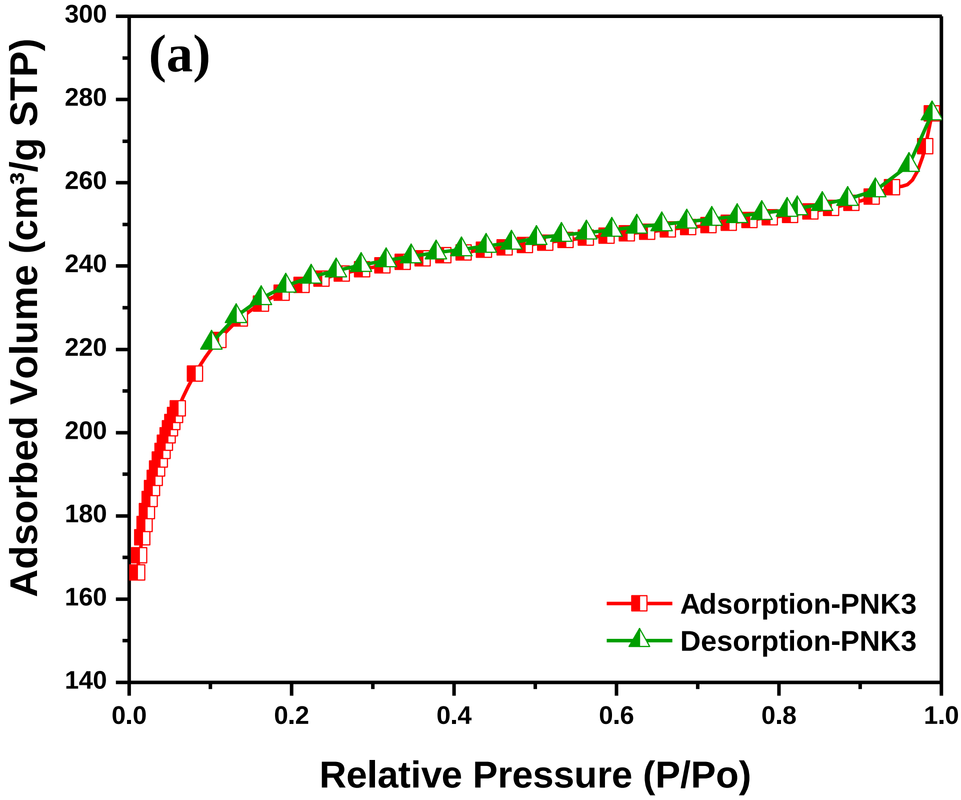


**Fig. 5.** $N_2$ adsorptions isotherms of selected ACs, peanut shell group (a and f); pine wood group (b and c) and walnut shell group (d and e).

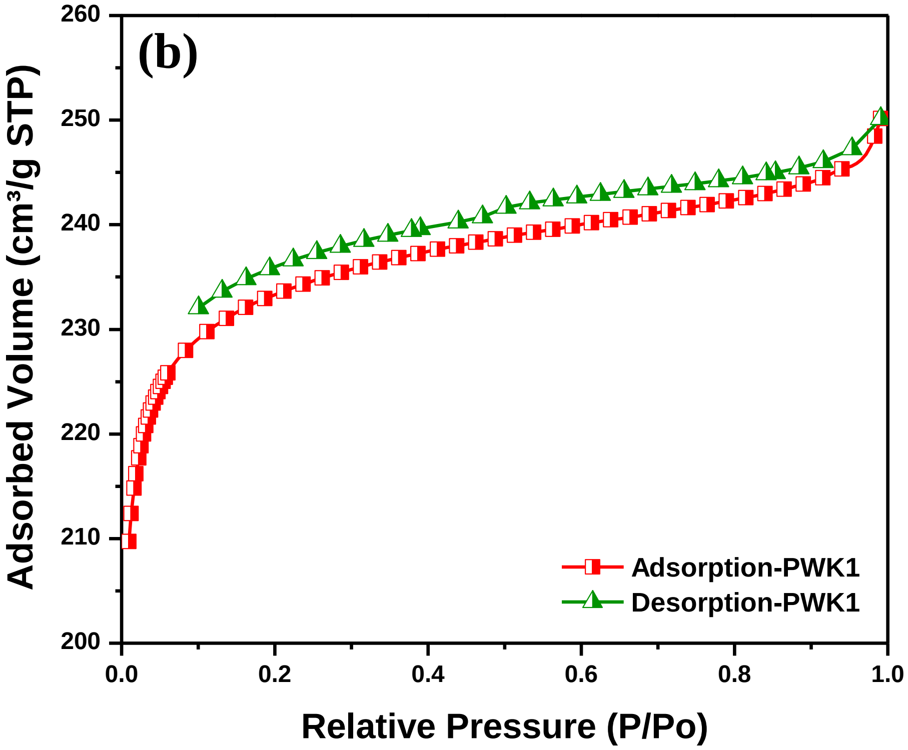


**Fig. 5.** $N_2$ adsorptions isotherms of selected ACs, peanut shell group (a and f); pine wood group (b and c) and walnut shell group (d and e).

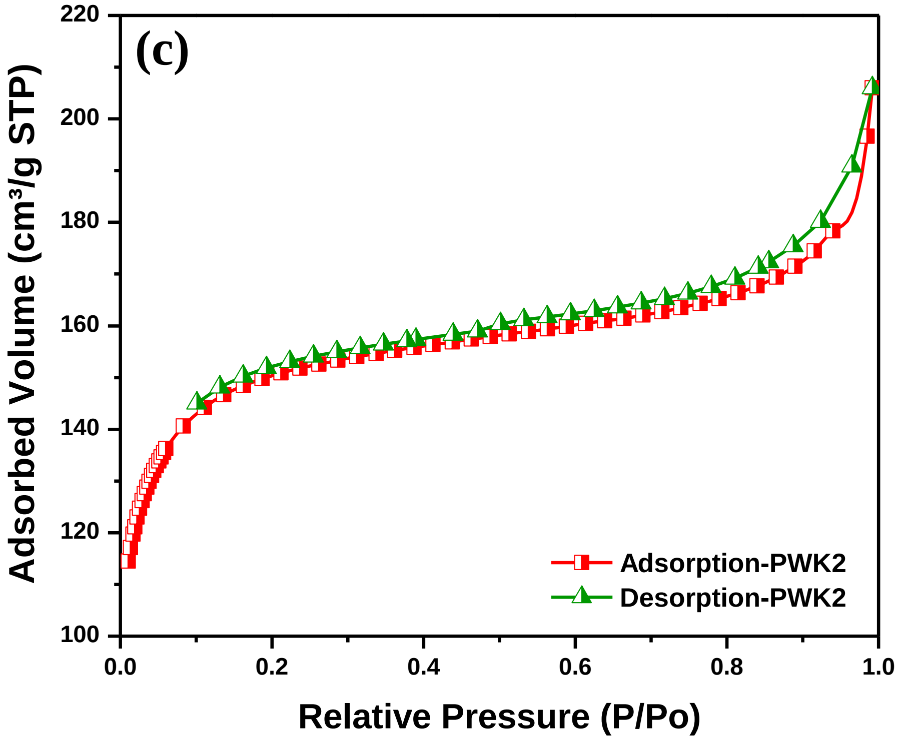


**Fig. 5.** $N_2$ adsorptions isotherms of selected ACs, peanut shell group (a and f); pine wood group (b and c) and walnut shell group (d and e).

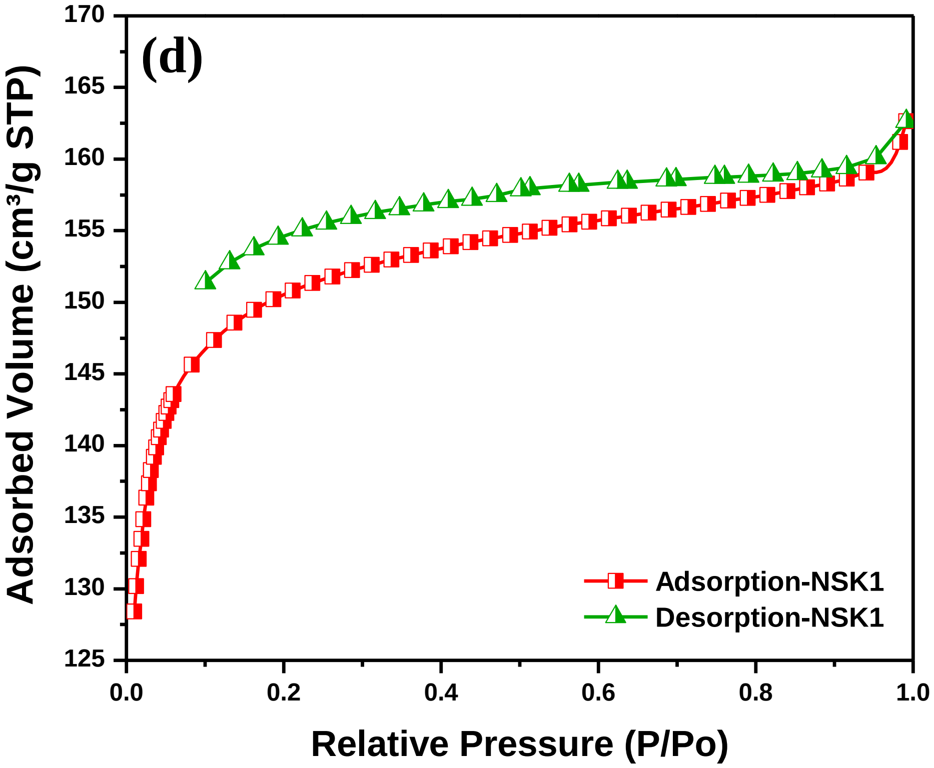


**Fig. 5.** $N_2$ adsorptions isotherms of selected ACs, peanut shell group (a and f); pine wood group (b and c) and walnut shell group (d and e).

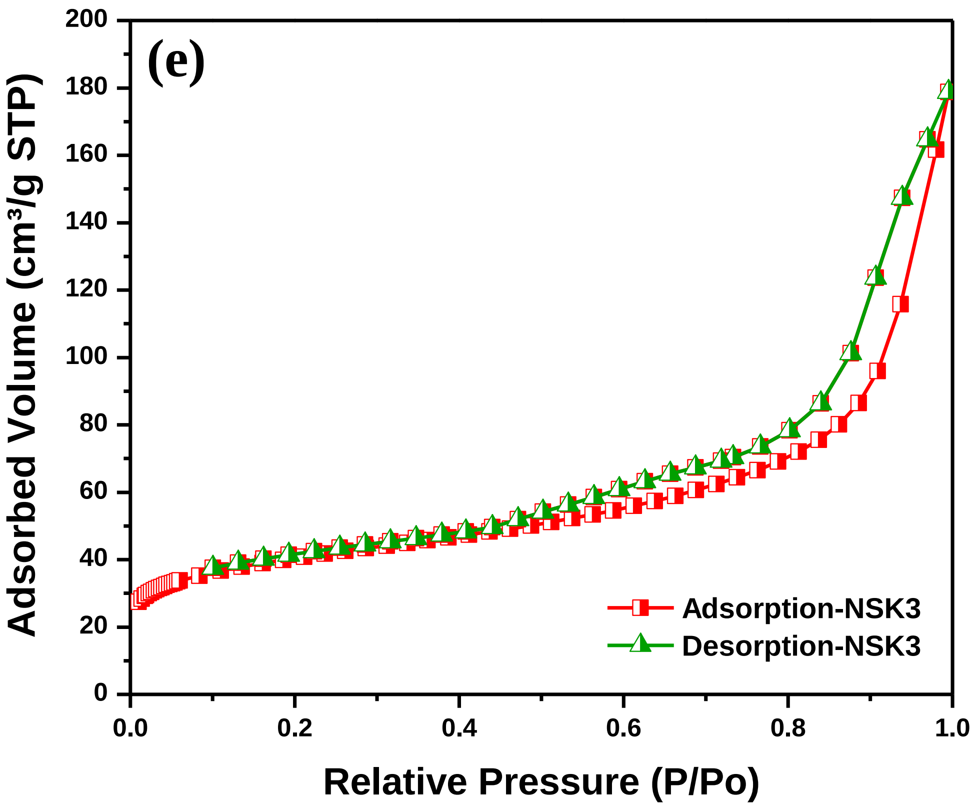


**Fig. 5.** $N_2$ adsorptions isotherms of selected ACs, peanut shell group (a and f); pine wood group (b and c) and walnut shell group (d and e).

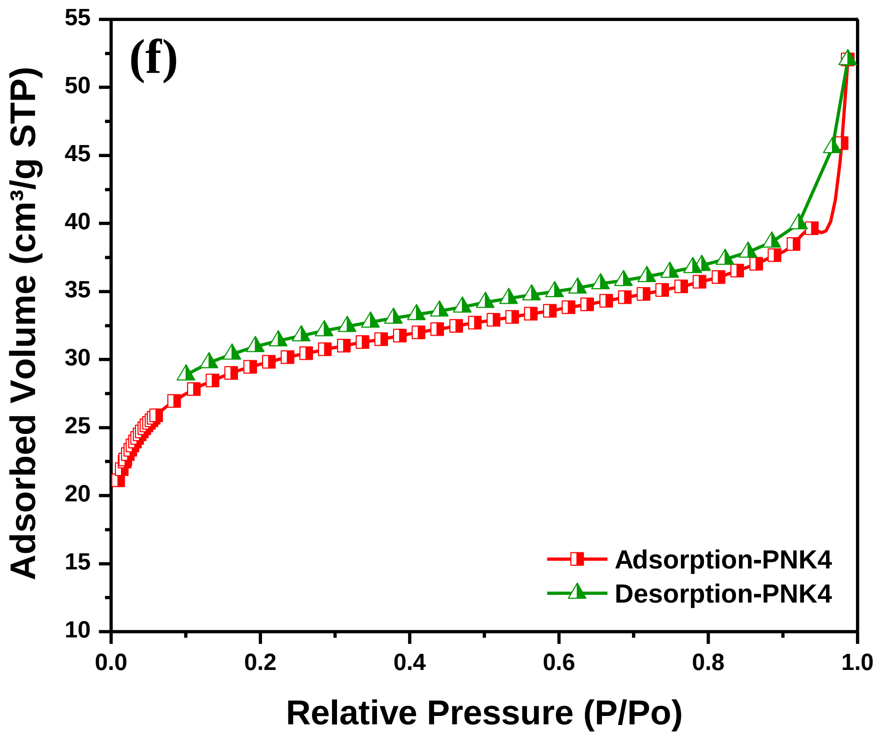


**Fig. 5.** $N_2$ adsorptions isotherms of selected ACs, peanut shell group (a and f); pine wood group (b and c) and walnut shell group (d and e).

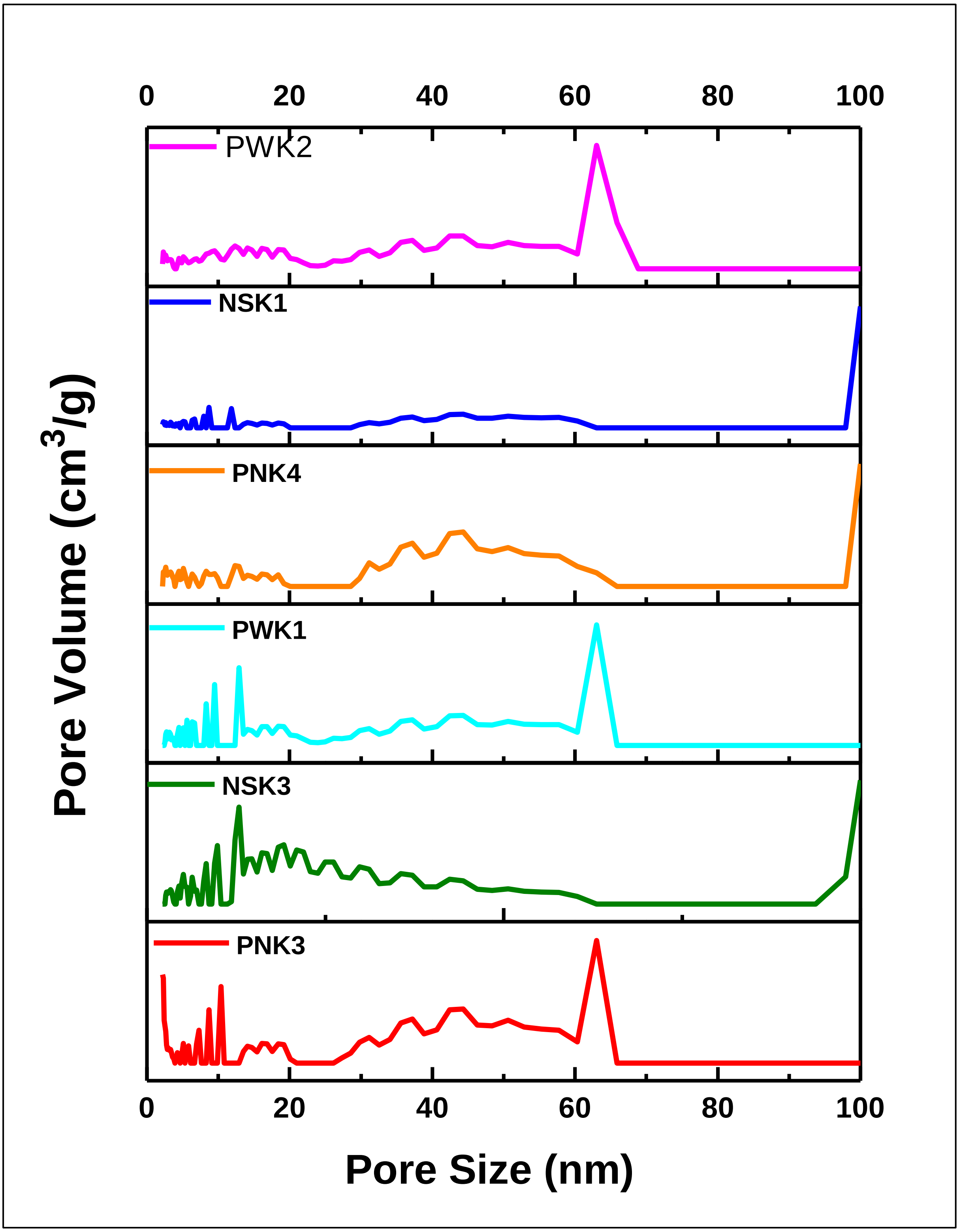


**Fig. 6.** Pore size distribution for selected samples from different groups of biomass.

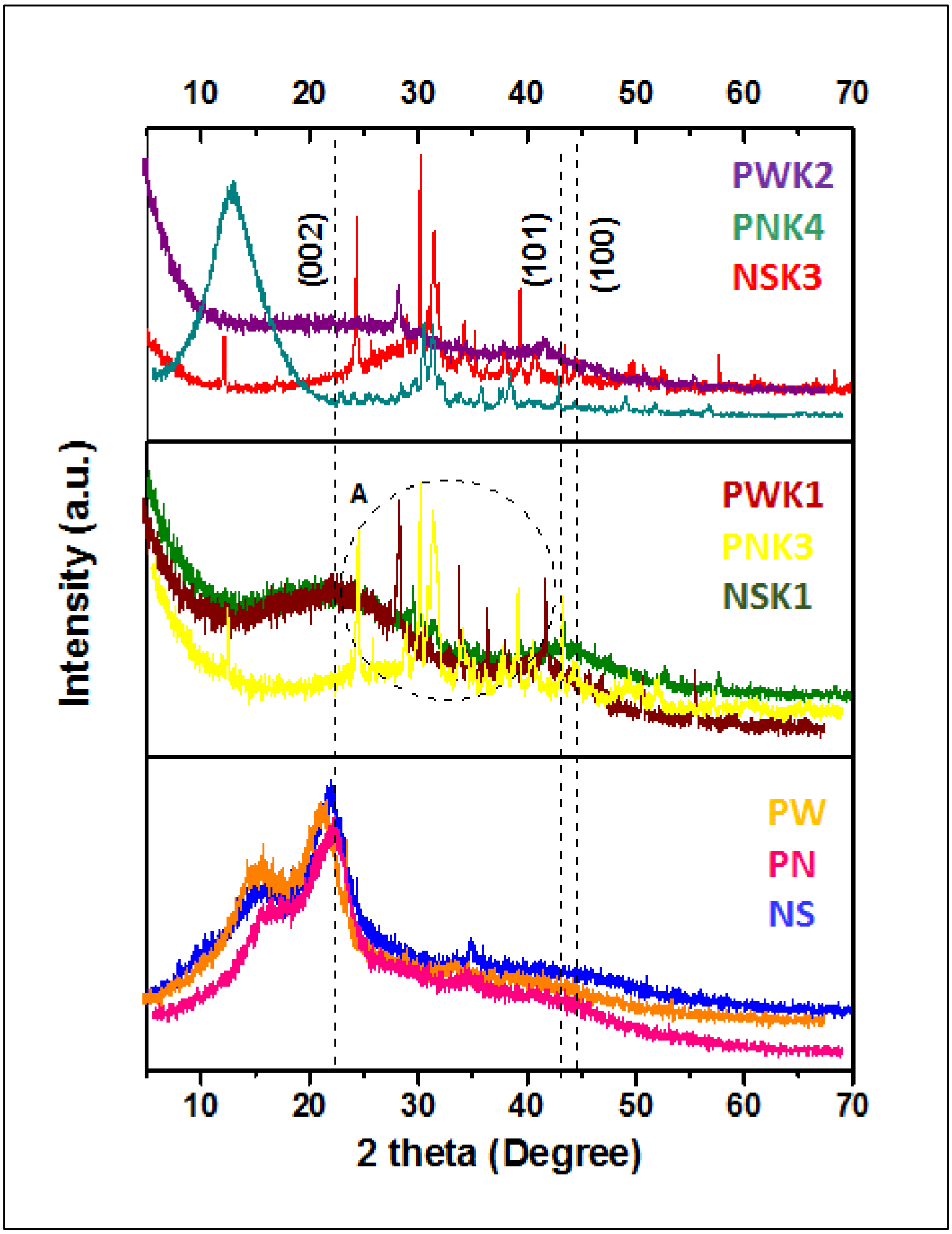


**Fig. 7.** XRD profile of walnut shell, peanut shell and pine wood derived non-activated precursor and activated carbons.

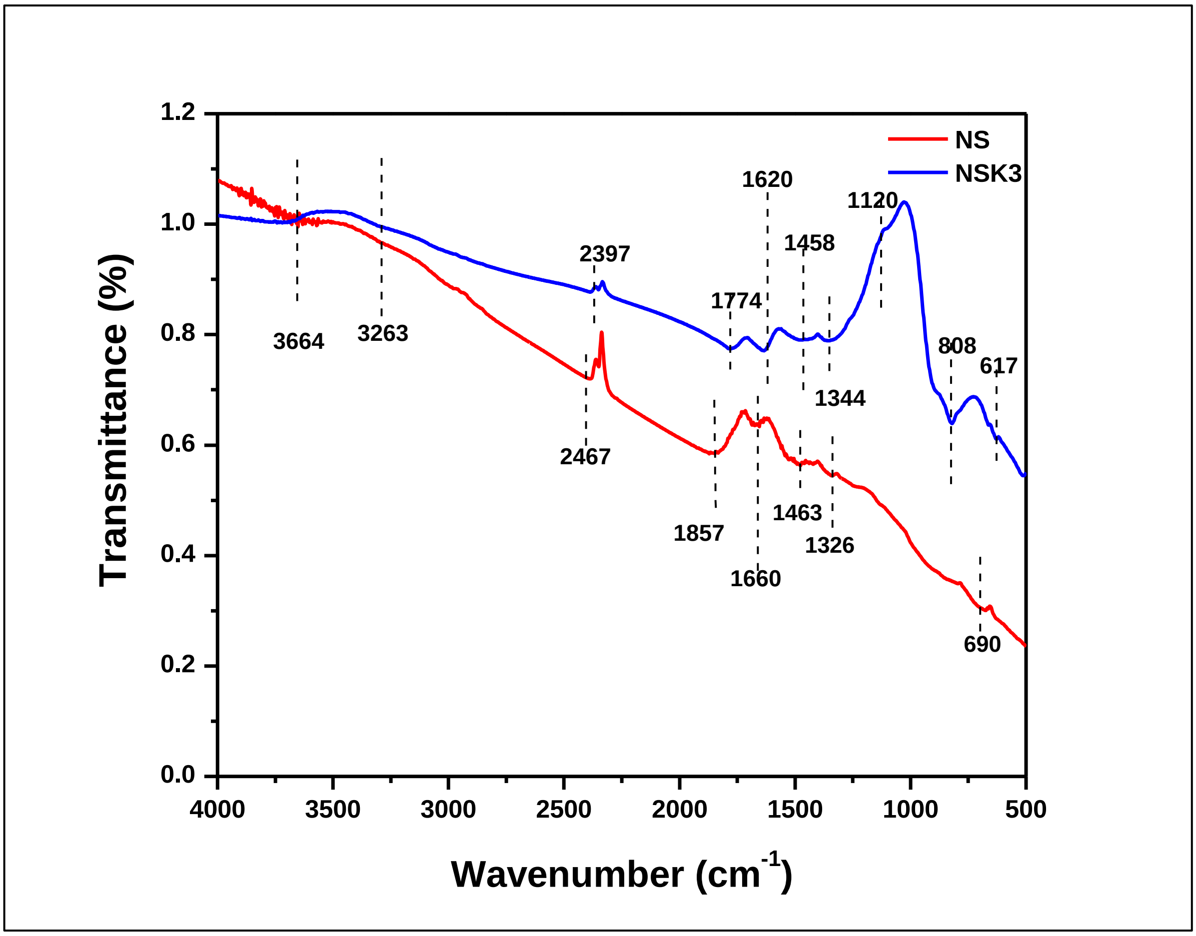


**Fig. 8.** FTIR spectra of walnut shell derived non-activated precursor and activated carbon.

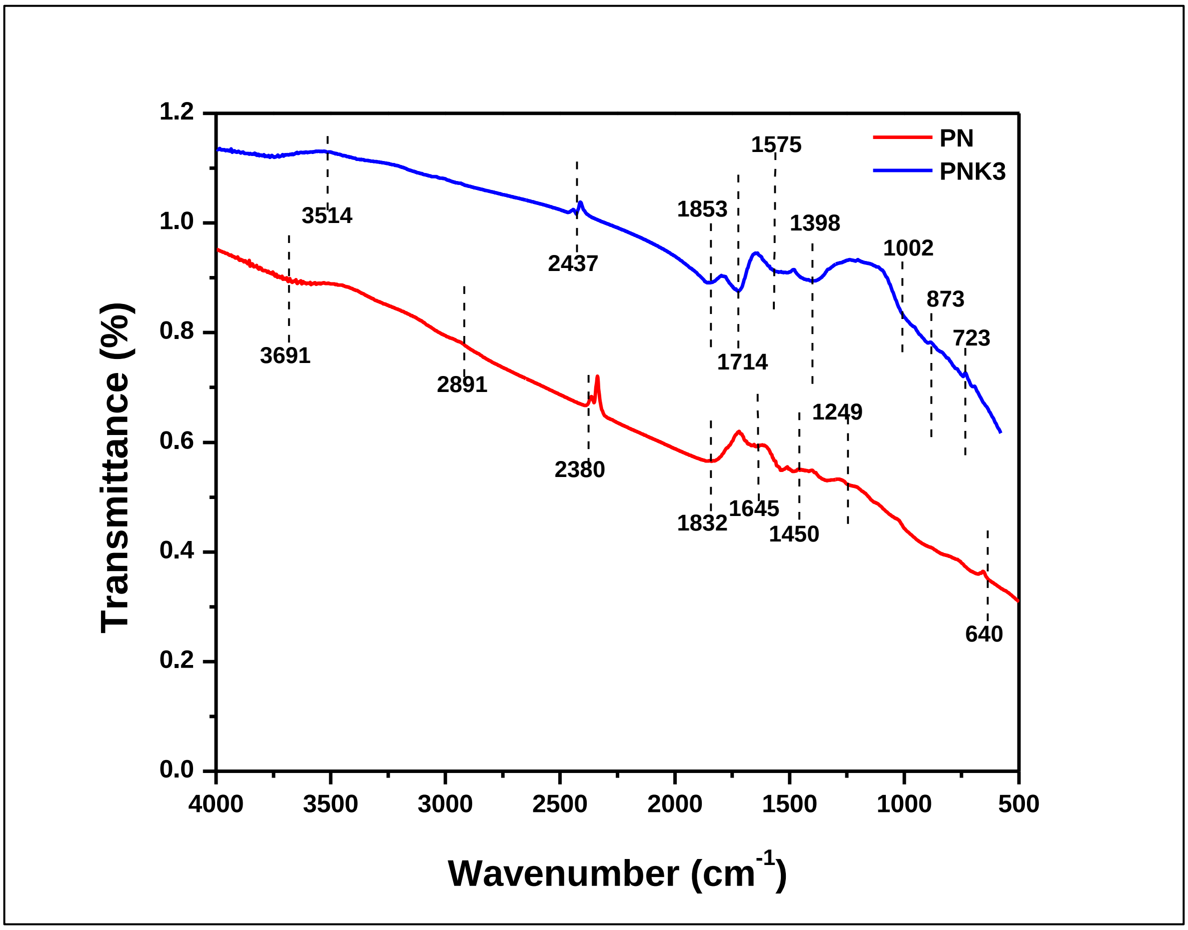


**Fig. 9.** FTIR spectra of peanut shell derived non-activated precursor and activated carbon.

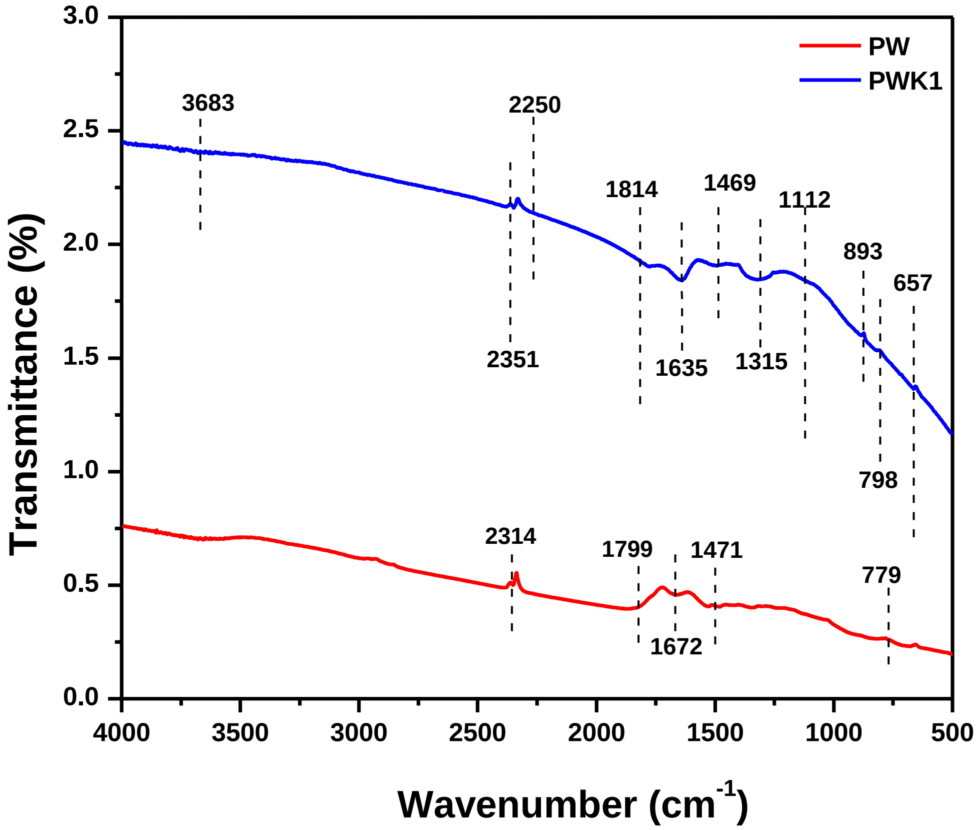


**Fig. 10.** FTIR spectra of pine wood derived non-activated precursor and activated carbon.

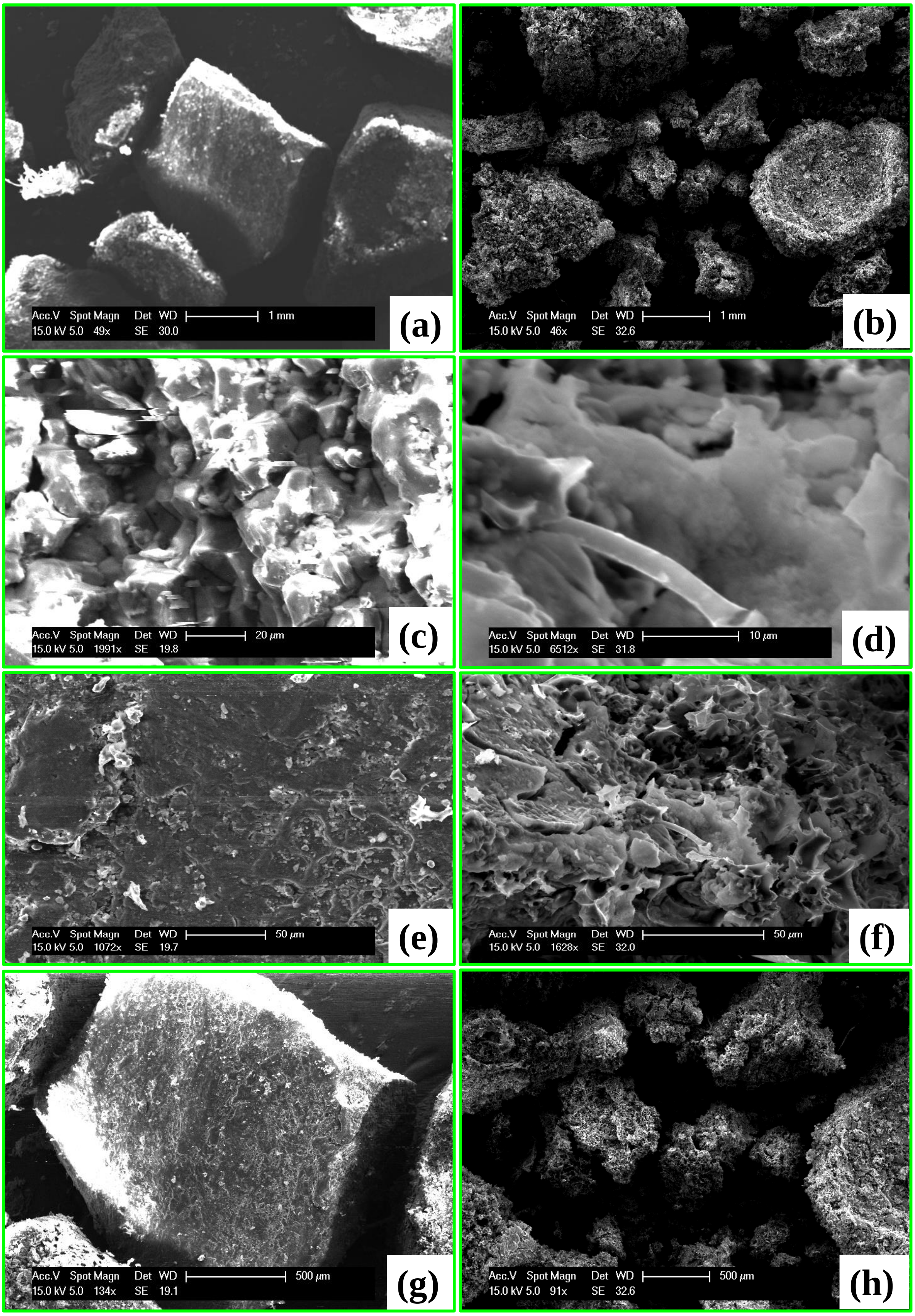


**Fig. 11.** SEM analysis of walnut shell derived non-activated: NS (a, c, e and g), and activated carbons: NSK3 (b, d, f and h).

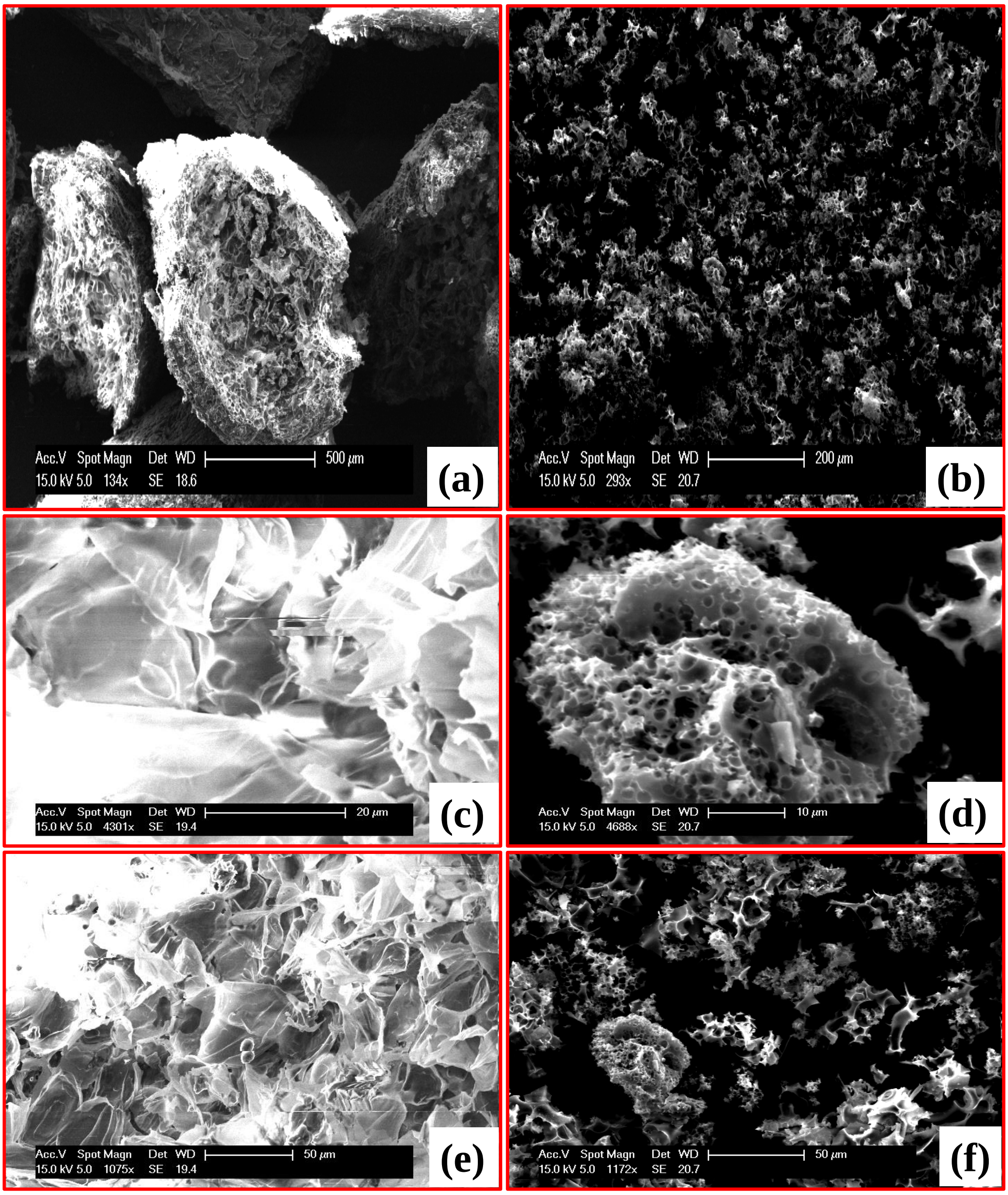


**Fig. 12.** SEM analysis of peanut shell derived non-activated: PN (a, c and e), and activated carbons: PNK3 (b, d and f).

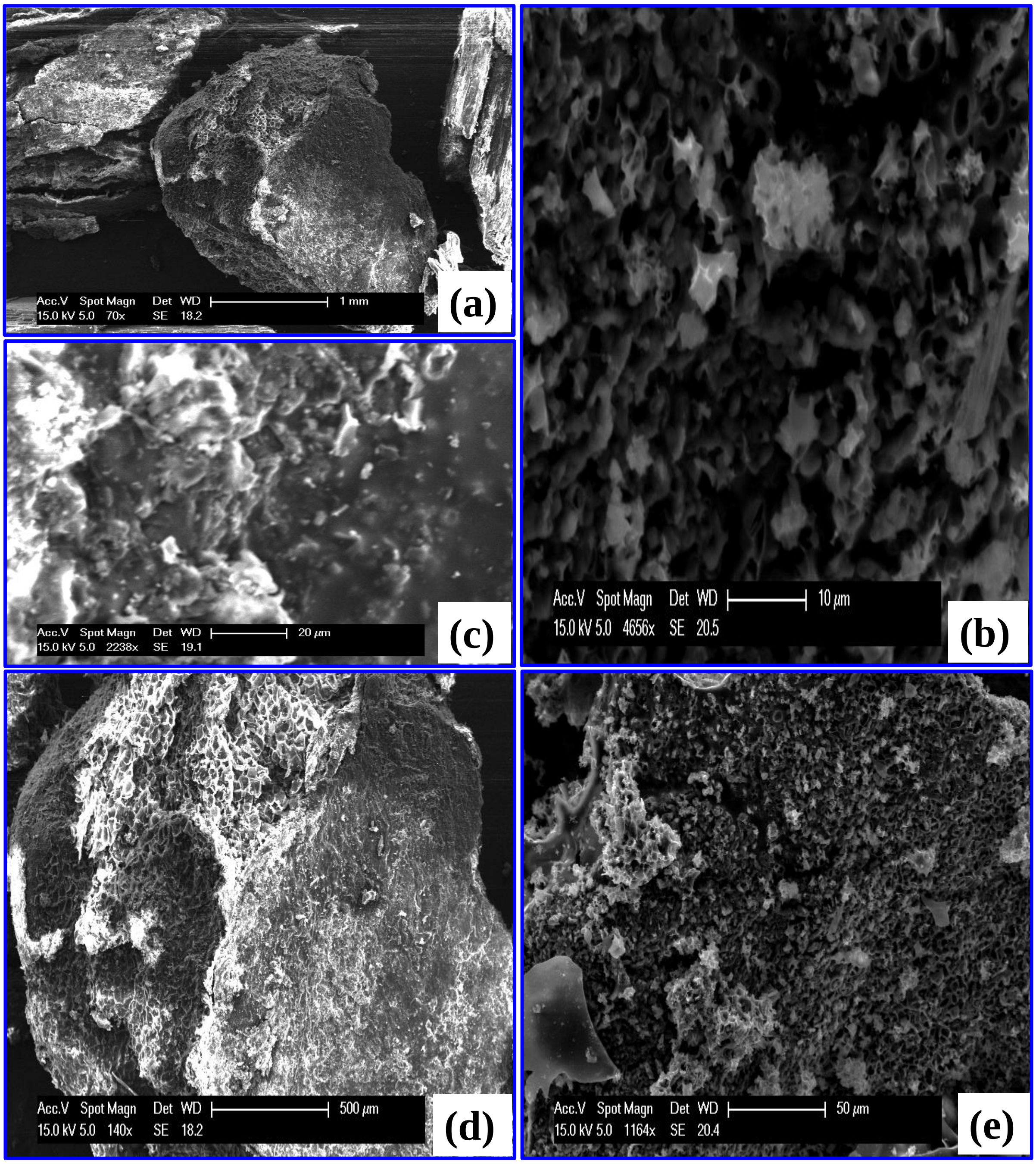


**Fig. 13.** SEM analysis of pine wood derived non-activated: PW (a, c and d), and activated carbons: PWK1 (b and e).